EUROPEAN ORGANISATION FOR NUCLEAR RESEARCH

CERN-PPE/94-105
14th July 1994

Measurement of Single Photon Production in e^+e^- Collisions near the Z^0 Resonance

The OPAL Collaboration

Abstract

A measurement of the single photon production cross-section is presented based on a data-sample of 40.5 pb^{-1} collected with the OPAL detector at centre-of-mass energies within 3 GeV of the Z^0 mass. Single photon events arise from initial state radiation and the production of an "invisible" final state consisting of neutrinos or possibly particles such as sneutrinos or photinos. The single photon topology is also sensitive to new Z^0 decays such as $Z^0 \to \bar{\nu}\nu^* \to \bar{\nu}\nu\gamma$ or $Z^0 \to \gamma X$, $X \to$ invisible particles. A total of 447 single photon candidates were observed with energy exceeding 1.75 GeV in the polar angle region $|\cos\theta| < 0.7$. The estimated background from processes with visible reaction products, mainly $e^+e^- \to e^+e^-\gamma$, is 37 ± 6 events. Interpreting the cross-sections as being solely due to Z^0 decay to invisible particles and the expected W-contributions, the Z^0 invisible width is determined to be $539 \pm 26 \pm 17$ MeV corresponding to $N_\nu = 3.23 \pm 0.16 \pm 0.10$ light neutrino generations. The differential cross-section with photon energy is presented. Upper limits are set on additional invisible contributions to the Z^0 width, on possible non-resonant processes, and on Z^0 decays to single photons. The energy spectra are used to constrain exotic sources of high energy single photons. In particular, the radiative two-body decay of the Z^0 to a new particle X, with mass below 64 GeV and an invisible signature, has a Z^0 branching ratio of less than 4.3×10^{-6} at 95 % confidence level.

Submitted to Z. Phys. C.

The OPAL Collaboration

R. Akers[16], G. Alexander[23], J. Allison[16], K.J. Anderson[9], S. Arcelli[2], S. Asai[24], A. Astbury[28], D. Axen[29], G. Azuelos[18,a], A.H. Ball[17], E. Barberio[26], R.J. Barlow[16], R. Bartoldus[3], J.R. Batley[5], G. Beaudoin[18], A. Beck[23], G.A. Beck[13], J. Becker[10], C. Beeston[16], T. Behnke[27], K.W. Bell[20], G. Bella[23], P. Bentkowski[18], S. Bentvelsen[8], P. Berlich[10], S. Bethke[32], O. Biebel[32], I.J. Bloodworth[1], P. Bock[11], H.M. Bosch[11], M. Boutemeur[18], S. Braibant[12], P. Bright-Thomas[25], R.M. Brown[20], A. Buijs[8], H.J. Burckhart[8], C. Burgard[27], P. Capiluppi[2], R.K. Carnegie[6], A.A. Carter[13], J.R. Carter[5], C.Y. Chang[17], C. Charlesworth[6], D.G. Charlton[8], S.L. Chu[4], P.E.L. Clarke[15], J.C. Clayton[1], S.G. Clowes[16], I. Cohen[23], J.E. Conboy[15], M. Coupland[14], M. Cuffiani[2], S. Dado[22], C. Dallapiccola[17], G.M. Dallavalle[2], C. Darling[31], S. De Jong[13], H. Deng[17], M. Dittmar[4], M.S. Dixit[7], E. do Couto e Silva[12], J.E. Duboscq[8], E. Duchovni[26], G. Duckeck[8], I.P. Duerdoth[16], U.C. Dunwoody[5], P.A. Elcombe[5], P.G. Estabrooks[6], E. Etzion[23], H.G. Evans[9], F. Fabbri[2], B. Fabbro[21], M. Fanti[2], M. Fierro[2], M. Fincke-Keeler[28], H.M. Fischer[3], P. Fischer[3], R. Folman[26], D.G. Fong[17], M. Foucher[17], H. Fukui[24], A. Fürtjes[8], P. Gagnon[6], A. Gaidot[21], J.W. Gary[4], J. Gascon[18], N.I. Geddes[20], C. Geich-Gimbel[3], S.W. Gensler[9], F.X. Gentit[21], T. Geralis[20], G. Giacomelli[2], P. Giacomelli[4], R. Giacomelli[2], V. Gibson[5], W.R. Gibson[13], J.D. Gillies[20], J. Goldberg[22], D.M. Gingrich[30,a], M.J. Goodrick[5], W. Gorn[4], C. Grandi[2], P. Grannis[8], E. Gross[26], J. Hagemann[27], G.G. Hanson[12], M. Hansroul[8], C.K. Hargrove[7], J. Hart[8], P.A. Hart[9], M. Hauschild[8], C.M. Hawkes[8], E. Heflin[4], R.J. Hemingway[6], G. Herten[10], R.D. Heuer[8], J.C. Hill[5], S.J. Hillier[8], T. Hilse[10], D.A. Hinshaw[18], P.R. Hobson[25], D. Hochman[26], A. Höcker[3], R.J. Homer[1], A.K. Honma[28,a], R.E. Hughes-Jones[16], R. Humbert[10], P. Igo-Kemenes[11], H. Ihssen[11], D.C. Imrie[25], A. Jawahery[17], P.W. Jeffreys[20], H. Jeremie[18], M. Jimack[1], M. Jones[6], R.W.L. Jones[8], P. Jovanovic[1], C. Jui[4], D. Karlen[6], K. Kawagoe[24], T. Kawamoto[24], R.K. Keeler[28], R.G. Kellogg[17], B.W. Kennedy[20], B. King[8], J. King[13], S. Kluth[5], T. Kobayashi[24], M. Kobel[10], D.S. Koetke[8], T.P. Kokott[3], S. Komamiya[24], R. Kowalewski[8], R. Howard[29], P. Krieger[6], J. von Krogh[11], P. Kyberd[13], G.D. Lafferty[16], H. Lafoux[8], R. Lahmann[17], J. Lauber[8], J.G. Layter[4], P. Leblanc[18], P. Le Du[21], A.M. Lee[31], E. Lefebvre[18], M.H. Lehto[15], D. Lellouch[26], C. Leroy[18], J. Letts[4], L. Levinson[26], Z. Li[12], F. Liu[29], S.L. Lloyd[13], F.K. Loebinger[16], G.D. Long[17], B. Lorazo[18], M.J. Losty[7], X.C. Lou[8], J. Ludwig[10], A. Luig[10], M. Mannelli[8], S. Marcellini[2], C. Markus[3], A.J. Martin[13], J.P. Martin[18], T. Mashimo[24], P. Mättig[3], U. Maur[3], J. McKenna[29], T.J. McMahon[1], A.I. McNab[13], J.R. McNutt[25], F. Meijers[8], F.S. Merritt[9], H. Mes[7], A. Michelini[8], R.P. Middleton[20], G. Mikenberg[26], J. Mildenberger[6], D.J. Miller[15], R. Mir[26], W. Mohr[10], C. Moisan[18], A. Montanari[2], T. Mori[24], M. Morii[24], U. Müller[3], B. Nellen[3], B. Nijjhar[16], S.W. O'Neale[1], F.G. Oakham[7], F. Odorici[2], H.O. Ogren[12], C.J. Oram[28,a], M.J. Oreglia[9], S. Orito[24], J.P. Pansart[21], G.N. Patrick[20], M.J. Pearce[1], P. Pfister[10], P.D. Phillips[16], J.E. Pilcher[9], J. Pinfold[30], D. Pitman[28], D.E. Plane[8], P. Poffenberger[28], B. Poli[2], A. Posthaus[3], T.W. Pritchard[13], H. Przysiezniak[18], M.W. Redmond[8], D.L. Rees[8], D. Rigby[1], M. Rison[5], S.A. Robins[13], D. Robinson[5], J.M. Roney[28], E. Ros[8], S. Rossberg[10], A.M. Rossi[2], M. Rosvick[28], P. Routenburg[30], Y. Rozen[8], K. Runge[10], O. Runolfsson[8], D.R. Rust[12], M. Sasaki[24], C. Sbarra[2], A.D. Schaile[8], O. Schaile[10], F. Scharf[3], P. Scharff-Hansen[8], P. Schenk[4], B. Schmitt[3], H. von der Schmitt[11], M. Schröder[12], H.C. Schultz-Coulon[10], P. Schütz[3], M. Schulz[8], C. Schwick[27], J. Schwiening[3], W.G. Scott[20], M. Settles[12], T.G. Shears[5], B.C. Shen[4], C.H. Shepherd-Themistocleous[7], P. Sherwood[15], G.P. Siroli[2], A. Skillman[16], A. Skuja[17], A.M. Smith[8], T.J. Smith[28], G.A. Snow[17], R. Sobie[28], R.W. Springer[17], M. Sproston[20], A. Stahl[3],

C. Stegmann[10], K. Stephens[16], J. Steuerer[28], B. Stockhausen[3], R. Ströhmer[11], D. Strom[19], P. Szymanski[20], H. Takeda[24], T. Takeshita[24], S. Tarem[26], M. Tecchio[9], P. Teixeira-Dias[11], N. Tesch[3], M.A. Thomson[15], S. Towers[6], T. Tsukamoto[24], M.F. Turner-Watson[8], D. Van den plas[18], R. Van Kooten[12], G. Vasseur[21], M. Vincter[28], A. Wagner[27], D.L. Wagner[9], C.P. Ward[5], D.R. Ward[5], J.J. Ward[15], P.M. Watkins[1], A.T. Watson[1], N.K. Watson[7], P. Weber[6], P.S. Wells[8], N. Wermes[3], B. Wilkens[10], G.W. Wilson[4], J.A. Wilson[1], V-H. Winterer[10], T. Wlodek[26], G. Wolf[26], S. Wotton[11], T.R. Wyatt[16], A. Yeaman[13], G. Yekutieli[26], M. Yurko[18], W. Zeuner[8], G.T. Zorn[17].

[1]School of Physics and Space Research, University of Birmingham, Birmingham B15 2TT, UK
[2]Dipartimento di Fisica dell' Università di Bologna and INFN, I-40126 Bologna, Italy
[3]Physikalisches Institut, Universität Bonn, D-53115 Bonn, Germany
[4]Department of Physics, University of California, Riverside CA 92521, USA
[5]Cavendish Laboratory, Cambridge CB3 0HE, UK
[6]Carleton University, Department of Physics, Colonel By Drive, Ottawa, Ontario K1S 5B6, Canada
[7]Centre for Research in Particle Physics, Carleton University, Ottawa, Ontario K1S 5B6, Canada
[8]CERN, European Organisation for Particle Physics, CH-1211 Geneva 23, Switzerland
[9]Enrico Fermi Institute and Department of Physics, University of Chicago, Chicago IL 60637, USA
[10]Fakultät für Physik, Albert Ludwigs Universität, D-79104 Freiburg, Germany
[11]Physikalisches Institut, Universität Heidelberg, D-69120 Heidelberg, Germany
[12]Indiana University, Department of Physics, Swain Hall West 117, Bloomington IN 47405, USA
[13]Queen Mary and Westfield College, University of London, London E1 4NS, UK
[14]Birkbeck College, London WC1E 7HV, UK
[15]University College London, London WC1E 6BT, UK
[16]Department of Physics, Schuster Laboratory, The University, Manchester M13 9PL, UK
[17]Department of Physics, University of Maryland, College Park, MD 20742, USA
[18]Laboratoire de Physique Nucléaire, Université de Montréal, Montréal, Quebec H3C 3J7, Canada
[19]University of Oregon, Department of Physics, Eugene OR 97403, USA
[20]Rutherford Appleton Laboratory, Chilton, Didcot, Oxfordshire OX11 0QX, UK
[21]CEA, DAPNIA/SPP, CE-Saclay, F-91191 Gif-sur-Yvette, France
[22]Department of Physics, Technion-Israel Institute of Technology, Haifa 32000, Israel
[23]Department of Physics and Astronomy, Tel Aviv University, Tel Aviv 69978, Israel
[24]International Centre for Elementary Particle Physics and Department of Physics, University of Tokyo, Tokyo 113, and Kobe University, Kobe 657, Japan
[25]Brunel University, Uxbridge, Middlesex UB8 3PH, UK
[26]Particle Physics Department, Weizmann Institute of Science, Rehovot 76100, Israel
[27]Universität Hamburg/DESY, II Institut für Experimental Physik, Notkestrasse 85, D-22607 Hamburg, Germany
[28]University of Victoria, Department of Physics, P O Box 3055, Victoria BC V8W 3P6, Canada
[29]University of British Columbia, Department of Physics, Vancouver BC V6T 1Z1, Canada
[30]University of Alberta, Department of Physics, Edmonton AB T6G 2J1, Canada
[31]Duke University, Dept of Physics, Durham, NC 27708-0305, USA
[32]Technische Hochschule Aachen, III Physikalisches Institut, Sommerfeldstrasse 26-28, D-52056 Aachen, Germany

[a]Also at TRIUMF, Vancouver, Canada V6T 2A3

1 Introduction

Decays of the Z^0 can result in the pair production of neutral weakly interacting particles with mass less than $\frac{1}{2}m_Z$. The existence of a substantial Z^0 branching ratio into such "invisible" final states (≈ 20 %) has been inferred from precision measurements of the production cross-sections of hadrons and charged leptons in centre-of-mass energy scans near the Z^0 resonance [1, 2]. The total width of the Z^0, Γ_Z, measured from the lineshape width is some 500 MeV larger than can be accounted for by the visible width of the charged leptons and quarks measured from the pole cross-section. This indirect measurement of the invisible width, $\Gamma_{\rm inv}$, is of high precision. It is consistent with the Standard Model expectation for three light neutrino generations and can be interpreted as a measurement of $N_\nu = 2.980 \pm 0.027$ [1, 2, 3], where N_ν is the effective number of light neutrino generations deduced from the Z^0 invisible width based on the expected partial width for one light neutrino generation ($N_\nu = \Gamma_{\rm inv}/{\Gamma_\nu}^{SM}$). Within the Standard Model, with three light neutrino species, $\Gamma_{\rm inv}$ is expected to be 500.8 ± 2.6 MeV for $m_Z = 91.187$ GeV and $m_{\rm top}$ in the range 100 to 200 GeV [4].

In this paper we directly measure the production cross-section of events with invisible particles. Such events, expected to be predominantly due to Z^0 decays to invisible particles, are observable when a photon radiated from an initial state lepton is the only particle detected by the experiment, thus signalling an annihilation to an invisible final state. This direct method of determining $\Gamma_{\rm inv}$ was recognised by many authors [5]. It is statistically less precise than the indirect one but is complementary in many respects. In particular, the indirect method depends on measuring all visible decays, even exotic ones. Single photon events can also arise within the Standard Model from t-channel W exchange yielding electron-type neutrinos. Together with the interference of the W diagram with the Z^0 exchange diagrams, these W contributions are expected to reduce the single photon cross-section at the Z^0 peak by about 8 %. At higher energies, the single photon cross-section measurement can probe the W-W-γ coupling [6], however this contribution is expected to be small near the Z^0 mass.

Single photon measurements have been made at lower energy e^+e^- colliders [7] and at LEP, initially by OPAL [8] and later also by L3 and ALEPH [9]. The average of all previous LEP measurements is $N_\nu = 2.97 \pm 0.17$. These results agree with the Standard Model expectation for three light neutrinos and also with the indirect measurements.

New physics processes, such as production of additional heavy neutrinos, or other weakly interacting particles, such as sneutrinos [10], could lead to non-integral values of the measured N_ν. Mechanisms such as the existence of right-handed neutrinos which mix with their left-handed counterparts [11] could reduce N_ν. Thus precise measurements of N_ν are needed to address such models.

The single photon topology also constitutes a very simple experimental signature which can be used to set model independent upper limits on the production cross-section. These upper limits are relevant to the production of several new particles, such as neutralinos, single excited neutrinos, variant axions [12], technicolour inspired pseudo Goldstone bosons [13] and gravitinos [14]. Many searches for particular particles using the single photon topology appear in the literature [7], [15]. The lower energy searches are complementary since "background" from Z^0 decay to invisible particles is heavily suppressed.

In this paper, we explore possible Z^0 decays to single photons and constrain possible non-resonant sources of single photons such as $e^+e^- \to \gamma\tilde{\gamma}\tilde{\gamma}$. The fully corrected differential cross-section with photon energy is presented and compared with the expectation for $\nu\overline{\nu}\gamma(\gamma)$ production. We also search for the production, in association with a photon, of a new particle (invisible or with invisible decay modes), by examining the recoil mass distribution of the photon.

The relevant aspects of the OPAL detector are described in section 2. The selection of single photon event candidates, and the estimation of the efficiency of this event selection are described in sections 3 and 4 respectively. The background from various processes with visible reaction products is estimated in section 5 and checked in section 6. The efficiency estimate is based on measurements from the data with control samples. The background is mainly estimated by Monte Carlo simulation of known background processes, and it is checked with data by relaxing some of the selection criteria. The results on the total cross-section are presented in section 7. The interpretation of these results within the Standard Model is described in section 8, while in the next section we derive limits on new physics contributions. In section 10, we present the differential cross-section with photon energy, which is both compared to the expectation from $e^+e^- \to \nu\overline{\nu}\gamma(\gamma)$ and is used to set model independent limits on exotic sources of single photons.

2 OPAL detector

The OPAL detector, described in detail in [16], is a detector with a pressurised central tracking system operating in a 0.435 T axial magnetic field. The lead-glass electromagnetic calorimeter together with presamplers and time-of-flight (TOF) scintillators is located outside the magnet solenoid and pressure vessel. The magnet return yoke is instrumented for hadron calorimetry and is surrounded by external muon chambers. Electromagnetic calorimeters close to the beam axis[1] measure luminosity and complete the acceptance. The detector features of relevance to this analysis are described briefly below.

The central tracking system operates at a gas pressure of 4 bar and consists of a vertex drift chamber, a jet chamber and z-chambers. For data recorded after 1990, the vacuum chamber in the central region was made of beryllium and reduced to a radius of 5.3 cm, and a silicon micro-vertex detector [17] was installed at a radius of about 6 cm immediately outside this inner beam-pipe. The polar angle coverage of the tracking detectors is such that at least 20 points are measured in the jet chamber for charged tracks in the range $|\cos\theta| < 0.963$. Tracks with $|\cos\theta| < 0.97$ are measured with at least five hits in the vertex drift chamber. The probability of a photon conversion occurring in the material of the beampipe and the central tracking detector is about 8% in the barrel region for data recorded after 1990.

Most photons ($\approx 80\%$) incident on the material of the pressure vessel and magnet coil (1.8 radiation lengths at normal incidence) in the barrel region, convert and are therefore detected in the TOF and barrel presampler detectors located in front of the lead-glass calorimeter. The TOF detector consists of 160 scintillator counters forming a barrel of mean radius 2.36 m. Each counter is 6.8 m long (in z), and light is collected from both ends. The time of arrival of a photon is measured with a resolution of better than 300 ps. The presence of a signal in this

[1] A spherical polar co-ordinate system is used with the polar angle θ defined relative to the electron beam direction (z).

detector in coincidence with the barrel electromagnetic calorimeter means that a lower energy threshold can be used to accept single photon events in the trigger.

The energies of photons and electrons are measured by the barrel and endcap lead-glass electromagnetic calorimeters. These detectors provide full azimuthal coverage in the polar angle range of $|\cos\theta| < 0.82$ for the barrel and $0.81 < |\cos\theta| < 0.984$ for the endcaps. The forward detector electromagnetic calorimeters on both sides of the interaction point cover the polar angle region between 34 and 132 mrad. All three calorimeters provide sampling of the electromagnetic shower development over typically 24 radiation lengths for fiducially contained particles. When high energy electrons or photons are incident on the gap between the endcap lead-glass and the forward detector, some fraction of the shower is usually detected at the edge of one of these calorimeters. An additional electromagnetic calorimeter, called the gamma-catcher, fills this gap. It consists of a ring of lead-scintillator sandwich modules of seven radiation lengths thickness. The gamma-catcher was fully operational only for the data recorded in 1992. Thus, photons and electrons are detected with an acceptance of almost 4π.

The barrel lead-glass blocks have a pointing geometry. To achieve good hermeticity, the small 1 mm gaps between the lead-glass blocks do not point exactly to the interaction point. The blocks of the endcap calorimeter are arranged with their axes parallel to the beam direction. This means that the gaps do not point to the interaction point, and that particles from the interaction point typically deposit energy in several lead-glass blocks. Clusters are composed of contiguous blocks with at least one containing 20 (50) MeV for the barrel (endcap). Clusters are considered in the analysis if they have an energy exceeding 100 MeV. In the endcap region, only clusters with at least two blocks are considered. The cluster energies which are used correspond to the energy deposited in the active material (lead-glass) and have not been corrected for energy loss in the material in front of the calorimeter. The intrinsic energy resolution of the calorimeter is $5\text{–}6\%/\sqrt{E}$ which is degraded by about a factor of two by the material of the magnet coil and the pressure vessel.

The presence of muons is detected by the hadron calorimeters and muon detectors. This muon identification is used to veto events with muons originating from cosmic ray interactions or beam halo events[2], as well as e^+e^- collisions. In particular, the hadron pole-tip calorimeter extends the muon coverage to about $|\cos\theta| = 0.985$.

Single photon events in the barrel region are triggered by an inclusive trigger, based on the presence of at least one azimuthally matched coincidence between a TOF signal in an 18° half-angle azimuthal wedge and a corresponding signal in a trigger sector of the barrel electromagnetic calorimeter having more than about 700 MeV deposited energy. The electromagnetic component of the trigger is about 50 % efficient at 700 MeV, 90 % efficient at 1 GeV and fully efficient at 1.5 GeV. The trigger system is described in detail in [18].

3 Event selection

The analysis is designed to be efficient for low energy photons whilst keeping under control a number of backgrounds. The principal background to the $e^+e^- \to \nu\bar{\nu}\gamma(\gamma)$ signal is radiative

[2]Muons produced by interactions of off-momentum beam particles with the vacuum chamber.

Bhabha scattering, $e^+e^- \to e^+e^-\gamma$ where the photon is detected at wide angle and the electrons remain undetected at low angles close to or within the beam-pipe. In an hermetic detector such as OPAL, this type of background can be controlled with a minimum transverse energy requirement, of order 1 GeV, on the wide angle photon in conjunction with a calorimetric veto on additional significant energy deposits. In addition "instrumental backgrounds" arising from cosmic-ray muon interactions, muons from the beam halo, or interactions of beam particles with residual gas in, or with the wall of, the vacuum chamber must be considered.

The event selection criteria will be described in four stages :

- Neutral topology : require no charged tracks
- Photon acceptance/trigger definition
- Isolation (calorimetric vetoes)
- Background suppression

The first two stages define the acceptance of the analysis and its efficiency. The isolation criteria are essential for rejecting several sources of physics background. Lastly the background suppression criteria are designed to remove residual instrumental backgrounds. The criteria build on those adopted in our previous publication [8].

Events are selected as single photon candidates if they satisfy all of the following criteria.

Neutral topology

- [N1] Charged track veto. Events are required to have no tracks reconstructed in the central detector with 20 or more jet chamber hits assigned to them. This removes events with a charged track with transverse momentum above about 100 MeV in the polar angle region $|\cos\theta| < 0.963$.

Acceptance

- [A1] Angular acceptance. The electromagnetic cluster with the highest deposited energy in the barrel and endcap calorimeters must be in the region $|\cos\theta| < 0.7$.
- [A2] Coil conversion. The above electromagnetic cluster must be matched within 50 mrad in azimuth by a TOF counter signal of good quality[3].
- [A3] Timing. The measured arrival time of the photon at the TOF must be within 2 ns of the expected time for a photon originating from the interaction point.
- [A4] Minimum energy. The deposited energy associated with the above electromagnetic cluster must exceed 1.5 GeV. All electromagnetic clusters within a 200 mrad half-angle cone of the first cluster are included in the energy sum. A photon with true energy of 1.75 GeV deposits about 1.5 GeV of energy in the calorimeter after traversing the coil.

[3]Timing information from both ends of the scintillation counter is required.

- [A5] Trigger. The event must satisfy the TOF-electromagnetic barrel coincidence trigger which is a sufficient condition for the event to be recorded.

Isolation

The following calorimetric vetoes against significant energy deposits remove physics backgrounds :

- [C1] Second cluster veto. The event is rejected if there is another cluster, outwith the 200 mrad cone around the highest energy cluster[4], detected in either the barrel or endcap electromagnetic calorimeters with deposited energy exceeding 300 MeV.
- [C2] Forward calorimeter veto. The total energy deposited in each forward calorimeter must be less than 2 GeV.
- [C3] Gamma-catcher veto. The most energetic gamma-catcher cluster must have an energy of less than 5 GeV. (This criterion was applied to data recorded in 1992 only.)

The following criteria are designed to reduce background from events where the cone around the accepted cluster contains additional energy deposits – as expected for a π^0.

- [P1] Cone-mass. The invariant mass of the electromagnetic clusters within the 200 mrad half-angle cone is formed using the deposited energy of each cluster. The expected value of this mass for a low energy ($\approx$ 2 GeV) π^0 with at least one photon converting in the coil is about 100 MeV. Events where this mass is between 50 and 150 MeV are removed.
- [P2] Presampler match. If present, the presampler barrel cluster with the largest signal within a 400 mrad half-angle cone of the primary electromagnetic cluster must match the electromagnetic cluster to within 100 mrad.

Background suppression

- [B1] Hit veto. Backgrounds from beam-wall and beam-gas interactions are reduced by requiring that the event contains no vertex chamber sector with 5 or more hits and no jet chamber sector with 50 or more hits.

Additional redundancy in the rejection of backgrounds from cosmic-ray or beam-halo muon interactions is achieved with the following criteria. Such backgrounds are already cut down effectively by the timing requirement (criterion A3).

- [B2] Cluster extent. The primary electromagnetic cluster combined with any clusters contiguous with it must not extend more than 200 mrad (equivalent to more than five

[4] As defined in criterion A1.

lead-glass blocks) in the polar or azimuthal directions. Muons from external sources, with a wide range of incidence angles, tend to give large clusters within the pointing geometry of the barrel electromagnetic calorimeter.

- [B3] Muon veto. Events are rejected if there are any muon track segments reconstructed in the barrel or endcap muon chambers, or in the barrel, endcap or pole-tip hadron calorimeters. Events are also rejected if three or more of the outer 8 layers of the barrel hadron calorimeter have strips hit in any 45 degree azimuthal road.

- [B4] Strip veto. The number of strips hit in any of the hadron calorimeter barrel or endcap sectors must be less than 5.

Summary

Events were selected from a data-sample of 40.5 pb^{-1} integrated luminosity collected from 1990 to 1992 within which all the main detector components used in the analysis were fully operational. A total of 447 single photon candidate events were selected.

4 Efficiency estimation

The selection efficiency for events from the $\mathrm{e^+e^-} \rightarrow \nu\overline{\nu}\gamma(\gamma)$ process is estimated from the full detector simulation [19] using the event generator based on the calculations in [20]. The detector response was simulated for events where at least one photon satisfied $E_\gamma > 0.5$ GeV ; $|\cos\theta| < 0.75$. Particularly important components of the efficiency are checked with data control samples, and where appropriate the efficiency estimate is corrected. The overall selection efficiency is estimated to be 65.7 ± 1.7 % for events within the chosen kinematic acceptance of $E_\gamma > 1.75$ GeV ; $|\cos\theta| < 0.7$. This efficiency is defined as

$$N_{\mathrm{selected}}/N_{\mathrm{generated}}$$

where $N_{\mathrm{generated}}$ is the number of events with at least one photon generated with $E_\gamma > 1.75$ GeV ; $|\cos\theta| < 0.7$, and N_{selected} is the number of events from the $\nu\overline{\nu}\gamma(\gamma)$ process accepted by the selection criteria and includes events which, due to resolution effects ("feed-through"), lie outside the $E_\gamma > 1.75$ GeV ; $|\cos\theta| < 0.7$ region. The measured cross-sections are based on this kinematic acceptance and are corrected for the expected effects of doubly radiative events ($\nu\overline{\nu}\gamma\gamma$).

In the following paragraphs we discuss the efficiency of each criterion in turn and, where appropriate, correct for observed discrepancies with the Monte Carlo (MC) description. The selection criteria described in section 3 have been listed in an order which roughly reflects the chronological order of the photon's passage through the detector, in order to reduce correlations among different criteria and facilitate comparison with data control samples. The efficiency of each criterion, which is listed later in Table 2, is after requiring all previous criteria.

Efficiency of the charged track veto (N1)

This criterion removes events where the photon converts in the beam-pipe or in the volume of the central detector up to a radius of about 1.65 m. The thickness of this material is evaluated to be 8.8 % of a radiation length at normal incidence, based on knowledge of the material composition. This is expected to have a fractional uncertainty of less than 10 %. The studies described in [21] indicate that the photon conversion rate is understood at about this level. The estimated inefficiency for the 1991 and 1992 data is 7.7 ± 0.8 %. Before the 1991 data-taking period, the silicon micro-vertex detector and inner beam-pipe (corresponding to 1.25% of a radiation length of material at normal incidence) were added to the detector. It is estimated that 1.1 % of all photons convert in this material. The estimated inefficiency for the 1990 data is therefore 6.6 ± 0.7 %.

Angular acceptance (A1)

The angular acceptance criterion, $|\cos\theta| < 0.7$, was extensively studied in the OPAL $e^+e^- \to e^+e^-$ analysis [1] for beam energy electrons. No correction was deemed necessary and an uncertainty of 0.12 % was assigned. Additional uncertainties in this analysis arise from the less precise polar angle measurement for low energy photons and from not correcting for the slight shift in the longitudinal coordinate of the average interaction point (at most a 0.2 % effect). We assign an error of 0.3 %.

Efficiency of the photon conversion requirement (A2)

In essence, this criterion requires that the photon converts in the material in front of the TOF. A control sample of 4272 isolated photons from the reactions $e^+e^- \to \ell^+\ell^-\gamma(\ell = e, \mu)$, $e^+e^- \to \gamma\gamma$ and radiative Bhabha scattering with one electron detected in the forward calorimeter, $e^+e^- \to (e)e\gamma$, was selected. The photon was required to be isolated by at least 200 mrad in azimuth from any track and to be detected within the $|\cos\theta| < 0.7$ region. The energy and polar angle distributions of the three samples are in good agreement with the MC expectation. The measured efficiencies for associating a TOF hit are shown in Table 1 together with the MC expectation. The three separate estimates are consistent and indicate an efficiency in the control sample of 80.8 ± 0.6 % which is somewhat higher than the 79.0 ± 0.5 % expected from MC. For increasing angles of incidence, and hence more traversed material, the efficiency increases in agreement with the shape expected from MC. The TOF association efficiency is expected to be fairly independent of the photon energy. A variation of about ± 2 % is expected in the range of 1.75 GeV up to the beam energy, arising mostly due to the effects of shower fluctuations at low energy. The energy dependence is checked over a wide range with the $\ell^+\ell^-\gamma$ sample and also the beam energy photons in the $\gamma\gamma$ sample and is found to be in good agreement with expectation. We elect to apply a correction factor to this component of the efficiency of 1.022 ± 0.015. The assigned error takes into account the statistical error on the check (0.010) and the level of agreement of the three control samples. The corrected efficiency for photons from the $e^+e^- \to \nu\overline{\nu}\gamma(\gamma)$ process is 80.0 ± 1.2 %.

Event type	Data (%)	MC (%)
$\ell^+\ell^-\gamma$	80.4 ± 0.7	78.0 ± 0.6
$\gamma\gamma$	83.5 ± 1.2	81.6 ± 0.8
(e)eγ	76.3 ± 2.4	80.4 ± 1.4
All	80.8 ± 0.6	79.0 ± 0.5

Table 1: Measured probability for a photon to convert in the coil or pressure vessel for each photon control sample compared to the MC expectation.

TOF timing (A3)

The efficiency of the TOF timing criterion, $|t_0| < 2$ ns, where t_0 is the measured arrival time minus the arrival time expected for a photon originating from the interaction point at the same polar angle, is estimated using photons from the control sample described above. The photons are required to satisfy criterion A2. The efficiency is found to be 99.45 ± 0.12 % while the $\nu\overline{\nu}\gamma(\gamma)$ MC estimate is 99.91 ± 0.03 %. We therefore apply a correction factor of 0.995 and assign a systematic error of 0.2 %.

Energy scale and resolution (A4)

The acceptance changes by approximately 1 % per 10 MeV uncertainty on the deposited energy scale at 1.5 GeV. Uncertainties on the energy scale are expected to arise principally from the detector calibration and the modelling of the energy loss in the upstream material. We check the energy scale with two samples. Firstly, we "calibrate" the energy scale at low energy with a high statistics sample of isolated electrons. Secondly we check whether the energy scale measured with a low statistics sample of photons is consistent with the observations with electrons.

The sample of single electron events arises from radiative Bhabha scattering ($e^+e^- \to e^+e^-\gamma$) and two-photon production of e^+e^- ($e^+e^- \to e^+e^-e^+e^-$). With this sample one can check the energy scale against the more precisely known momentum scale. The single electron event selection procedure is very similar to that described in our previous paper [8]. A sample of 43,103 low energy single electron events was selected with electron momenta in the range $1.0 < p < 3.0$ GeV and $|\cos\theta| < 0.7$ from the 40.5 pb^{-1} data-sample. The observed momentum and angular distributions of the single electrons are well described by the expectations from the two processes. We study the distribution of "energy loss" defined as $p - E$ where p represents the momentum measured by the central detector and E is the deposited energy associated with the electron in the electromagnetic calorimeter defined similarly to criterion A4 above. The energy loss distribution is fitted with a Gaussian distribution for several bins in p and $|\cos\theta|$ for data and MC. The fitted means are shown as a function of p and $|\cos\theta|$ in Figures 1 (a) and (b) respectively. The mean energy loss for data is between 20 and 30 MeV higher than that for MC for almost all of the bins. This shift shows little dependence on p or $|\cos\theta|$. The shift is estimated to be 25 ± 2 MeV for electrons which deposit energies of around 1.5 GeV ($p \approx 1.8$ GeV). The momentum scale itself is estimated to contribute an uncertainty of at most 6 MeV to this check where the estimate includes scale uncertainties as indicated from studies of the reconstructed K^0_s mass and uncertainties on the material thickness which affect electrons via bremsstrahlung in the central detector volume.

Secondly, we check the energy scale for low energy photons with a sample of radiative di-lepton events ($e^+e^- \to \ell^+\ell^-\gamma(\ell = e, \mu)$). The energy of the photon (and each lepton) can be fitted using the measured angles of all three particles and the kinematic constraints of four-momentum conservation. A sample of 705 radiative di-lepton events was selected where the photon has a fitted energy between 1 and 3 GeV. The selected photons are required to convert in the coil (criterion A2). The event selection requires that the angles of both tracks are well measured and that the photon is relatively well isolated (200 mrad in azimuth) from each lepton. Several criteria are required which reduce substantially any contamination from non-planar events and events with multiple photons. The photon energy is estimated on an event-by-event basis with a precision of typically 1 % for genuinely 3-body planar events. This error is negligible compared to the experimental resolution on the measured energy at low energy (about 10 %).

As in the study with single electrons we define the "energy loss" as $E_{\rm fit} - E$ where $E_{\rm fit}$ is the fitted (reference) energy and E is the deposited energy associated with the photon. The mean energy loss for the photon sample is about 100 MeV less than observed with the electron sample, as expected from the differences in shower development between electrons and photons. The $E_{\rm fit}$ and angular distributions of the data are described satisfactorily by the MC samples. The energy loss distributions observed for data and MC are fitted with a distribution[5] consisting of two half-Gaussians of different width. The fitted mean energy loss is larger in the data by 24 ± 12 MeV. Various alternative estimation methods with the same data-sample lead to data $-$ MC differences consistent with the above to within 10 MeV. The reference energy scale from the kinematic constraints, $E_{\rm fit}$, is estimated to have a systematic uncertainty of about 6 MeV arising from multiple photon effects. This check with photons in radiative di-lepton events indicates a difference in energy loss between data and MC ($24 \pm 12 \pm 12$ MeV) which is consistent with that observed with single electrons ($25 \pm 2 \pm 6$ MeV).

We elect to "calibrate" the deposited energy scale of the MC by shifting the deposited energy by -25 MeV as established using single electron data. We assign a systematic uncertainty on the energy scale of 15 MeV at 1.5 GeV (1 %) which leads to a 1.5% systematic uncertainty on the acceptance. The assigned uncertainty includes uncertainties associated with inferring the photon energy scale from the electron energy scale. The cross-check with photons is consistent with the electron study and has a precision comparable to the quoted systematic error. Including the energy scale shift, we estimate that 88.6 % of photons within the kinematic acceptance will have deposited energy above 1.5 GeV, while the number of selected photons is augmented by a factor of 1.094 due to feed-through from outside the kinematic acceptance. Both factors have been decreased by 1.3 % as a result of the energy scale shift. Uncertainties in the modelling of the energy resolution can also affect these factors. Based on the energy resolution measured with the electron and photon control samples, we assign an additional systematic uncertainty on the acceptance of 0.8 %.

[5]The need for an asymmetric distribution is a result of the measured energy of photons which convert late in the coil being higher than on average. Given that little energy is then lost in the coil, they are also subject to less fluctuation.

Trigger efficiency (A5)

Events satisfying selection criteria A1–A4 almost necessarily satisfy this trigger. The electromagnetic barrel and TOF components of the trigger efficiency are evaluated using 20,000 independently triggered single electron events. The overall trigger efficiency for single photon events passing criteria A1–A4 is estimated to be 99.9 ± 0.1 %.

Occupancy probability

Several of the event selection criteria, namely N1, C1–C3, B1, B3–B4, are vetoes on additional activity in the detector. The probability of a noise event, with characteristics satisfying some of the veto conditions, occurring per bunch crossing was estimated for each centre-of-mass energy and data-taking year using an unbiased bunch crossing trigger of fixed lower frequency. The occupancy probabilities per bunch crossing are estimated to be 2.79 ± 0.06 %, 3.60 ± 0.03 % and 2.72 ± 0.02 % for the 1990, 1991, and 1992 data-taking periods, respectively, based on 894,000 unbiased triggers. About one third of this inefficiency is related to coincident muons, mostly of cosmic-ray interaction origin, while the remainder is predominantly due to interactions of off-momentum beam-particles with the vacuum pipe ("beam-wall"). We estimate a systematic error of 0.5 % to account for uncertainties associated with the time and luminosity variation of the occupancy probability.

Multiple radiation

The calorimetric vetoes, C1–C3, may eliminate doubly-radiative neutrino production ($\nu\overline{\nu}\gamma\gamma$) if the second photon is detectable. The MC predicts that 3.0% of $\nu\overline{\nu}\gamma(\gamma)$ events are removed by these criteria. Experimental uncertainties related to the efficiency of detecting the second photon are small. The theoretical uncertainty on the rate of doubly radiative events is assessed as 0.3 % as indicated by comparisons in [22],[23] of the $\nu\overline{\nu}\gamma(\gamma)$ generator [20] and the KORALZ generator [24] for centre-of-mass energies near the Z^0. We assign a total systematic error of 0.4 %.

Other sources of inefficiency

The other criteria introduce little additional inefficiency. The π^0 rejection criteria (P1 and P2) are estimated from MC to have a small inefficiency of 0.5 % due to fluctuations in the lateral development of the photon shower. These two criteria have been studied with single electron events. In both cases the distributions of the cut variable agree qualitatively with expectation from MC, but somewhat more single electrons in the data fail the criterion than expected. Using the observations with single electrons as a guide, we increase the single photon inefficiency from 0.5 % to 0.8 % and assign a systematic error of 0.3 %.

The simulated response of the muon barrel detector includes noise hits, leading to a predicted 0.5 % inefficiency from criterion B3. However, given that noise hits are already accounted for

in the occupancy probability, we assign full efficiency to this criterion. The tracking chamber hit vetoes[6] (B1), the cluster extent criterion (B2) and the hadron calorimeter strip vetoes (B4) introduce negligible inefficiency. The latter criterion has a minor inefficiency of 0.1 % due to fluctuations in the longitudinal shower development which occasionally lead to strip hits in the first layer. Checks with single electrons indicate that such mechanisms are indeed small. Nevertheless we assign a systematic error of 0.1 %.

Efficiency summary

The estimated selection efficiency for $\nu\overline{\nu}\gamma(\gamma)$ events with a photon in the $E_\gamma > 1.75$ GeV; $|\cos\theta| < 0.7$ region is summarised in Table 2. The actual efficiency estimated for each centre-of-mass energy varies somewhat from this average efficiency due to small variations of the occupancy probability with time and the absence of the inner material associated with the silicon micro-vertex detector in the 1990 data.

Criterion	Correction factor	Efficiency (%)
N1 – No tracks	1.000 ± 0.008	92.3
A1 – $\|\cos\theta\| < 0.7$	1.000 ± 0.003	99.3
A2 – Associated TOF	1.022 ± 0.015	80.0
A3 – $\|t_0\| < 2$ns	0.995 ± 0.002	99.4
A4 – Deposited energy above 1.5 GeV	0.987 ± 0.008	88.6
A5 – Trigger	0.999 ± 0.001	99.9
C1–C3 Calorimetric vetoes	1.000 ± 0.004	97.0
P1,P2 π^0 vetoes	0.997 ± 0.003	99.2
B1-B4 Background suppression	1.005 ± 0.001	99.8
Feed-through	0.986 ± 0.008	109.4
Occupancy (typical)	0.970 ± 0.005	97.0
Total	0.961 ± 0.024	65.7 ± 1.7

Table 2: Estimated selection efficiency for photons with $E_\gamma > 1.75$ GeV ; $|\cos\theta| < 0.7$. The efficiency is evaluated using the $\nu\overline{\nu}\gamma(\gamma)$ generator and includes the listed correction factors to account for observed deficiencies of the simulation. The efficiency of each criterion is given after applying the previous criteria. The deposited energy scale has been shifted by -25 MeV as described in the text. The feed-through represents the 9.4 % increase in "efficiency" arising from photons which do not originate within the above kinematic acceptance but were selected due to the finite resolution of the polar angle measurement and especially the energy measurement. The energy scale shift and its uncertainty affect criterion A4 and the feed-through in a correlated manner. The corresponding systematic errors have been added linearly.

5 Background estimate

Events with a single photon topology can be produced by several physics processes which give rise to a photon and visible reaction products. The event selection is sensitive to such

[6] Photon conversions resulting in reconstructed tracks in the jet chamber are already removed by criterion N1.

backgrounds when all the visible reaction products escape detection either by remaining in or near the beam-pipe or by depositing an insignificant amount of energy in the electromagnetic calorimeters. The dominant background is radiative Bhabha scattering, $e^+e^- \to e^+e^-\gamma$. Other backgrounds, namely, $e^+e^- \to \gamma\gamma\gamma$, $e^+e^- \to \mu^+\mu^-\gamma$, $e^+e^- \to \tau^+\tau^-\gamma$, two-photon production of meson resonances with neutral decay modes ($\pi^0, \eta, \eta', f_2(1270)$) and two-photon production of electron or muon pairs with a radiated photon are also estimated. The uncertainty on the background estimate is dominated by our understanding of the radiative Bhabha scattering contribution as the other sources are either much smaller or relatively well understood ($\mu^+\mu^-\gamma$).

The background contributions are estimated using appropriate event generators and are based on a full simulation of the detector response [19] and the event reconstruction as in section 4. The corrections deemed necessary from studying various aspects of the efficiency, including the occupancy probability, are also applied to the background estimate. We use the TEEGG event generator [25] in lowest order to describe the radiative Bhabha scattering process. Fully simulated events were generated on the Z^0 resonance and the centre-of-mass energy dependence of the accepted event rate was estimated at the generator level. The $e^+e^- \to \gamma\gamma\gamma$ process was simulated using the generator described in [26]. Two-photon resonance production was simulated according to [27]. The latter background is dominated by π^0 production.

The other two-photon process $e^+e^- \to e^+e^-\ell^+\ell^-\gamma(\ell = e, \mu)$ was considered in [22]. The event generator for this process uses a combination of the exact lowest order calculation of $e^+e^- \to e^+e^-e^+e^-$ and $e^+e^- \to e^+e^-\mu^+\mu^-$ and a procedure [28] to add on a radiated photon to the lepton-pair from the two-photon interaction. The cross-section, relevant to our single photon event selection and estimated with this event generator and the full detector simulation, is 0.03 pb.

The background estimates from all the above processes were calculated at the Z^0 peak and were re-scaled[7] to the other centre-of-mass energies according to the energy dependence of the $e^+e^- \to e^+e^-\gamma$ cross-section which is approximately linear with a slope of about +8 % per GeV[8]. The contributions from the $e^+e^- \to \mu^+\mu^-\gamma$ and $e^+e^- \to \tau^+\tau^-\gamma$ processes, where the di-lepton predominantly arises from Z^0 decay, are estimated using KORALZ [24] and are evaluated at several centre-of-mass energies.

The background estimates for the various contributing processes are listed below in Table 3 together with their associated systematic uncertainty. Checks of the background processes, discussion of the backgrounds estimated from the data and justification of the assigned systematic errors are given in section 6. In addition to the simulated physics processes, contributions from cosmic-ray interactions and single beam interactions are included as estimated from the data. A systematic uncertainty of 2 events is included from possible additional backgrounds suggested by the study of events failing exclusively due to the tracking chamber hit vetoes. Lastly, based on the two events in the 1992 data vetoed solely by the gamma-catcher, we estimate the contribution from this unmodelled background in the pre-1992 data. The errors quoted on the background estimates for the simulated physics processes are the quadrature sum of the MC statistical error and the assigned systematic error. The systematic errors range from 10 %

[7] For the non-$e^+e^-\gamma$ backgrounds this choice of $\sqrt{s}$ dependence is not expected to be exactly correct; the much lower cross-section of these other backgrounds means, however, that this approximation is of little consequence.

[8] The cross-section increases with centre-of-mass energy because requirements are made on the photon energy rather than the scaled photon energy.

for the $\mu^+\mu^-\gamma$ and $\tau^+\tau^-\gamma$ contributions to 100 % for the $e^+e^-\ell^+\ell^-\gamma(\ell = e, \mu)$ contribution. The total error on the background is mostly determined by the 20 % systematic uncertainty assessed for the radiative Bhabha process.

Background process	Events expected
$e^+e^- \to e^+e^-\gamma$	17.6 ± 4.9
$e^+e^- \to \gamma\gamma\gamma$	2.3 ± 1.0
$e^+e^- \to e^+e^-X(X = \pi^0, \eta, \eta', f_2(1270))$	2.6 ± 1.8
$e^+e^- \to \mu^+\mu^-\gamma$	8.0 ± 1.4
$e^+e^- \to \tau^+\tau^-\gamma$	2.3 ± 0.6
$e^+e^- \to e^+e^-\ell^+\ell^-\gamma(\ell = e, \mu)$	0.8 ± 0.8
cosmic ray interactions	1.0 ± 1.0
beam-gas/beam-wall	1.0 ± 1.0
hit veto inefficiency	$0.0 + 2.0$
gamma-catcher region (pre-1992)	1.6 ± 1.1
Total	37.1 ± 6.2

Table 3: Number of events expected from each background process in the complete data-sample.

6 Background studies and systematic checks

In this section, we verify whether the number of events failing particular background rejection criteria is well described by the simulated signal and background processes. In cases where there is a significant disagreement which is considered likely to contaminate the signal sample, appropriate corrections or systematic errors are assigned. Backgrounds established from the data are also estimated. We identify a reasonably pure sample of the main background source, namely radiative Bhabhas, and check the rate against the prediction. For the other physics background sources it is not possible to isolate a pure and representative sample of background events, and the assigned systematic error takes into account both this ignorance and an estimate of the uncertainty on the generator cross-section.

Radiative Bhabha background

The radiative Bhabha background is rejected mainly by the forward calorimeter veto (C2). There are 751 events rejected by this veto compared to an expectation of 795 ± 23 from all the simulated MC processes. Most of the predicted events are from the $e^+e^- \to e^+e^-\gamma$ process but a significant fraction (≈ 10 %) are expected from $e^+e^- \to \gamma\gamma\gamma$. The energy of the most energetic forward detector hemisphere is shown in Figure 2. One sees that the shape and normalisation of the energy spectrum at low energy agree with expectation indicating that the analysis is insensitive to the exact value of the energy cut.

Following the practice adopted in [8], we check the absolute cross-section prediction with singly-tagged single photons. These are single photon candidates which fail the forward calorimeter veto (C2) on account of at least half the beam energy being measured in one forward detector

and less than 2 GeV in the other. The high forward detector energy requirement selects tagged particles which are fiducially contained in this calorimeter (scattering angles between 40 and 120 mrad). A total of 582 of the 751 events described above satisfy this more selective definition. The 582 observed events can be compared with an expectation of 654 ± 20 from the $e^+e^- \to e^+e^-\gamma$ and $e^+e^- \to \gamma\gamma\gamma$ processes. The deposited energy and signed $\cos\theta$ distributions for the barrel photon are shown in Figures 3 (a) and (b). The $\cos\theta$ distribution is signed positively when the tag is in the same hemisphere in z as the photon and negatively otherwise. The ratio of number of events observed to that expected is 0.89 ± 0.05.

Given that we rely heavily on the calorimetric vetoes to reject the radiative Bhabha background, we have checked the hermeticity of the detector in the forward region using events with a single electron detected in the barrel. We require a minimum transverse momentum of the electron candidate, which for three-body $e^+e^- \to e^+e^-\gamma$ events is sufficiently high to constrain kinematically at least one of the other two particles, assumed to be of beam energy, to be scattered by at least 34 mrad, corresponding to the effective veto angle of the forward detector. The single electron selection is very similar to that described in [8] and in particular requires criterion C1. Additional criteria reduce the $\tau^+\tau^-$ contamination. From a sample of 6004 single electron candidates all but 28 are vetoed by the forward detector. This is higher than the 5.4 ± 4 events expected from the modelled processes of $e^+e^- \to e^+e^-\gamma$, $e^+e^-e^+e^-$, $e^+e^-\mu^+\mu^-$, $e^+e^-\tau^+\tau^-$ (4 ± 4 events), $\tau^+\tau^-$ and $\nu\overline{\nu}\gamma(\gamma)$ (1.4 ± 0.4 events). The first four potential sources of these events have been simulated at only lowest order. In higher orders, topologies occur where the transverse momentum of the barrel electron is balanced by a particle with energy less than half the beam energy, emitted well above the 34 mrad forward detector veto angle. The absence of a response may be a genuine inefficiency to beam energy particles or perhaps a result of an inefficiency to lower energy particles associated with higher order processes.

The 28 events were visually examined. The majority have no activity, other than the track, which would exclude them from the single photon selection. Of the 14 events found in 1992, three events have a gamma-catcher cluster with energy in excess of 8 GeV opposite in azimuth to the observed electron which has $p_T < 4$ GeV. In all three events there is a second electromagnetic cluster close to the inner edge of the endcap which has a deposited energy only slightly below the second cluster veto threshold of 300 MeV. These events are not consistent with a three-body final state. The final single photon selection criteria include the gamma-catcher veto. Correcting for the three events, we find a possible veto inefficiency of 0.3 %. Based on this possible inefficiency of the forward veto, we assign a fractional systematic error of 13 % on the $e^+e^-\gamma$ background in the single photon selection. This is calculated based on 0.3 % of the number of single photon events vetoed exclusively by the forward detector (751).

As summarised in Table 4, the total systematic uncertainty on the background from the radiative Bhabha process is estimated to be 20 %. This includes uncertainty from the possible veto inefficiency and an 11 % uncertainty based on the comparison of the observed production rate of "tagged single photons" with expectation. Other contributions arise from the photon energy scale and resolution, the modelling of the forward detector veto at the inner edge, and the estimated influence of higher order corrections.

Systematic	Error (%)
Possible veto inefficiency	13
Tagged single photon check	11
Photon energy scale and resolution	7.5
Higher order corrections	5
Effective veto angle ($\pm$ 1 mrad)	5
Total	20

Table 4: Systematic errors on the $e^+e^- \to e^+e^-\gamma$ background estimate.

Systematic checks

Veto on additional electromagnetic clusters (C1)

A total of 420 events are removed exclusively by the second cluster veto. In 387 of these events both electromagnetic clusters have deposited energies exceeding half the beam energy in good agreement with the expectation of 413 ± 12 for the theoretically well understood $e^+e^- \to \gamma\gamma(\gamma)$ QED process. This tests the normalisation and several aspects of the efficiency.

We remove the gamma-catcher veto (C3) in order to evaluate its effectiveness. In the events vetoed by a lower second cluster energy, 18 events, compared to an expectation of 48 ± 5, have a second cluster at the inner edge of the endcap, $|\cos\theta| > 0.97$, with energy exceeding 1 GeV. Events in this region are expected to be mainly from $e^+e^- \to e^+e^-\gamma$ where one of the electrons scrapes the inner edge. It should be noted that all MC $e^+e^-\gamma$ events with electrons scattered by more than 34 mrad are rejected by the single photon selection. In order to study whether, as a result of an inefficiency of C1 near the endcap inner edge, some $e^+e^-\gamma$ events with electrons scattering above this veto angle have been selected as single photon candidates, we investigated using the gamma-catcher for the 1992 data. Ten of the 18 inner edge events were recorded in 1992. All ten had a gamma-catcher cluster with an energy of at least 15 GeV. Thus, use of the gamma-catcher for the 1992 data significantly improves the background rejection power in the overlap region between the forward detector and the endcap electromagnetic calorimeter. Of the 210 single photon candidates from 1992 selected without requiring criterion C3, two events have an energy deposit in the gamma-catcher exceeding 5 GeV. Both events have a soft ($E < 0.3$ GeV) energy deposit at the inner edge of the endcap calorimeter close in azimuth to the gamma-catcher cluster and opposite in azimuth to the barrel photon, which has a deposited energy of around 2 GeV. It is kinematically excluded that these two events result from a three-body process such as $e^+e^-\gamma$. In conclusion, the number of candidates vetoed by a second cluster of moderate energy near the endcap inner edge differs from MC expectation. However, no evidence is found for a significant contamination of the single photon sample from $e^+e^-\gamma$ events where one or more electron is scattered well above the veto angle. A significant hole in the veto for $e^+e^-\gamma$ events is already ruled out by studies with a much higher statistics sample of single electrons.

With all analysis criteria applied, twelve events are rejected solely because of a second electromagnetic cluster with energy below 1 GeV in agreement with expectation (10.2 ± 1.1) from $\nu\bar{\nu}\gamma\gamma$ (7.3 ± 0.7), other physics processes (1.4 ± 0.8) and random noise (1.5 ± 0.3). The energy of the second most energetic cluster is shown in Figure 4 for the selected single photon

candidates and these twelve events and is compared to the expectation from random noise and from the physics processes. Below 300 MeV in second cluster energy, the data agree with the expectation from random noise. Eighteen events have $0.2 < E < 0.3$ GeV which is consistent with the 11.2 events expected where the second cluster arises mainly from noise.

Vetoes against π^0's

Criteria P1 and P2 remove a total of 9 events compared to an expectation of 5.3 events for the signal and background processes. By themselves these cuts are not essential. However a substantial number of events (50 in total) fail these criteria in conjunction with the other isolation criteria (C1,C2,C3). This is expected of, for example, untagged production of $e^+e^- \rightarrow e^+e^-f_2(1270)$ and tagged production of $e^+e^- \rightarrow e^+e^-\pi^0$.

Tracking chamber hit vetoes (B1)

A total of 20 events are removed exclusively by criterion B1 whilst one expects 11.7 ± 2.7 events predominantly from beam backgrounds coincident with signal events ($8.5 \pm 0.3 \pm 2.4$) and also modelled processes such as hard bremsstrahlung of single electrons in the detector material. Events from the $e^+e^- \rightarrow e^+e^-\gamma\gamma$ process are also expected to play a role. The timing of all events is consistent within 1 ns with an e^+e^- interaction. All 20 events have been visually examined. Most of the events cannot be unambiguously interpreted. Many appear consistent with accidental coincidences, while in some the photon seems correlated to the tracking chamber activity. Two of the events have a very soft track segment which is matched in azimuth with the observed photon, and are consistent with being single electron events where almost all the energy of the initial electron has been radiated in the material of the beam-pipe or vertex chamber. One expects 1.7 ± 0.5 such events based on simulating the passage of 75,000 2 GeV electrons through the detector material. We use the single electron events to give an indication of the possible contamination of the single photon sample. The estimated contamination from single electrons is negligible (0.3 ± 0.1 events). A genuine excess of 8 events in the hit veto check, with the same characteristics as single electrons, implies 1.3 ± 0.5 events selected as single photons. We assign a systematic uncertainty of 2 events to the overall background estimate due to this possible contamination.

Instrumental backgrounds

The t_0 distribution for the 456 single photon candidates selected with criterion A3 relaxed is shown in Figure 5. Nine events with $|t_0| > 2$ ns are rejected by the timing criterion. Based on the t_0 distribution of the photon control sample one expects a few single photon candidates (2.5 ± 0.5) with $|t_0| > 2$ ns. More out-of-time events are found with early times as expected for beam related background components such as upstream beam-wall interactions or beam halo muons. Cosmic-ray interactions are expected to arrive uniformly in time and have a uniform acceptance for $|t_0| < 10$ ns. We estimate the contamination of the signal region $|t_0| < 2$ ns by cosmic-ray interactions as 1 ± 1 event based on the number of events with t_0 in the range $4 < t_0 < 8$ ns. As discussed in [8], an estimate of the longitudinal origin of the photon, assuming

it was produced within the beam-pipe in the same direction as the parent beam particle, can be constructed from the measured arrival time of the photon at the TOF scintillator and the polar angle of the electromagnetic cluster. From studies of the estimated longitudinal origin for the selected events, we estimate a background of 1 ± 1 event arising from single beam interactions.

7 Results

A total of 447 single photon candidates are selected with an estimated background of 37.1 ± 6.2 events. The distributions of deposited energy and $|\cos\theta|$ of the selected photons are shown in Figures 6–8 and are compared with the expected distributions from the background processes plus $\nu\overline{\nu}\gamma(\gamma)$ production for $N_\nu = 3$. The shapes of both distributions show the general behaviour expected for initial state radiation.

Year	$\sqrt{s}$ (GeV)	$\int \mathcal{L}dt$ (pb^{-1})	N_{obs}	N_{bkgd}	ε (%)	$\sigma^{\rm meas}_{\nu\bar{\nu}\gamma(\gamma)}$ (pb)	$\sigma^{SM}_{N_\nu=3}$ (pb)
	88.252	0.433	2	0.3	67.1	5.9 ± 4.9	3.21
	89.256	0.348	1	0.2	67.0	3.2 ± 4.3	4.58
	90.254	0.195	2	0.2	66.8	14.0 ± 10.9	7.00
1990	91.244	2.540	21	2.5	66.8	10.9 ± 2.7	12.00
	92.234	0.399	7	0.4	67.0	24.7 ± 9.9	23.69
	93.238	0.441	11	0.5	66.7	35.8 ± 11.3	44.33
	94.234	0.489	22	0.5	67.1	65.5 ± 14.3	55.37
	88.480	0.828	3	0.5	65.7	4.5 ± 3.2	3.46
	89.470	0.800	6	0.6	64.6	10.5 ± 4.7	5.00
	90.226	0.871	11	0.8	65.5	17.9 ± 5.8	6.91
1991	91.243	8.107	80	7.9	65.1	13.7 ± 1.7	12.00
	91.970	0.825	16	0.8	65.5	28.1 ± 7.4	19.51
	92.968	0.794	22	0.8	64.8	41.1 ± 9.1	38.79
	93.716	0.914	35	1.0	65.6	56.8 ± 9.9	51.72
1992	91.299	22.473	208	20.1	65.8	12.7 ± 1.0	12.42
Total		40.458	447	37.1			

Table 5: Observed number of single photon candidates at each centre-of-mass energy for each data-taking year. The table includes the integrated luminosity, number of expected background events, the selection efficiency and background subtracted cross-section. The quoted error on the cross-section is purely statistical. The efficiency varies slightly among data-points due to variations in the occupancy probability. The efficiency for 1991 and 1992 data is lower than in 1990 due to the addition of the silicon microvertex detector. Also given is the expected cross-section for $N_\nu = 3$ evaluated from the event generator.

The efficiency of the analysis within the kinematic acceptance of $E_\gamma > 1.75$ GeV ; $|\cos\theta| < 0.7$ has little dependence on the assumed shape of the energy spectrum or the angular distribution. High statistics MC studies with the $\nu\overline{\nu}\gamma(\gamma)$ generator do not indicate any significant variation in efficiency among centre-of-mass energies. This test is sensitive to the centre-of-mass energy dependence of both the energy spectrum and the multiple photon emission rate. The efficiency variation is less than 1.5 % which is negligible compared to the off-peak statistical error and is therefore neglected.

The number of single photon candidates selected at each centre-of-mass energy, the integrated luminosity, the number of expected background events, the selection efficiency and the measured cross-section after background subtraction are shown in Table 5. The quoted cross-section is for production of a photon with $E_\gamma > 1.75$ GeV ; $|\cos\theta| < 0.7$ with no restrictions against additional photons. The efficiency at each data-taking point includes the occupancy probability measured for the particular data-set. Possible variations of the coil conversion probability and the energy scale with data-taking point were studied and found to be negligible. The systematic uncertainties on the cross-section measurement are summarised in Table 6. Most of the contributions are related to the efficiency and have already been discussed in section 4. The overall normalisation uncertainty due to the luminosity measurement is 0.6 % as described in [1]. The subtracted background has some dependence on centre-of-mass energy and amounts to about 1.4 pb with a systematic uncertainty of about 0.2 pb. The cross-section at each centre-of-mass energy is therefore measured with a systematic uncertainty of 2.7 % plus typically 0.2 pb.

Systematic	Error(%)
Energy scale and resolution	1.7
Conversion in coil	1.5
No conversion in central detector	0.8
MC statistics	0.7
Integrated luminosity	0.6
Occupancy probability	0.5
Multiple radiation	0.4
Shower lateral fluctuations	0.3
Fiducial acceptance	0.3
TOF timing	0.2
Shower containment	0.1
Trigger efficiency	0.1
Total	2.7

Table 6: Summary of the experimental systematic errors related to the efficiency and normalisation of the single photon cross-section measurement within the kinematic acceptance of $E_\gamma > 1.75$ GeV ; $|\cos\theta| < 0.7$.

8 Interpretation and Standard Model parameter estimation

The measured cross-sections are shown in Figure 9. The cross-section is seen to increase by an order of magnitude from the lowest to the highest energy scan point. The cross-sections are compared with the expectations for $\nu\overline{\nu}\gamma(\gamma)$ production with $N_\nu = 2$, 3 and 4 as calculated using the $\nu\overline{\nu}\gamma(\gamma)$ generator described in [20]. Qualitatively one sees the expected centre-of-mass energy dependence of initial state radiation in association with the decay of the Z^0 into invisible particles. In particular, the data show no evidence for sizeable components from possible non-resonant sources nor the possible Z^0 decay to a single photon and invisible particle(s). In section 9 we shall discuss limits on such exotic sources of single photon events.

In order to compare the measured single photon cross-sections with the Standard Model (SM) expectations arising principally from Z^0 invisible decays, we express the cross-section for invisible particle production via Z^0 exchange at the reduced centre-of-mass energy squared, s', as

$$\sigma_0(s') = \frac{12\pi}{{m_Z}^2} \frac{s'\Gamma_e\Gamma_{inv}}{(s' - {m_Z}^2)^2 + s'^2{\Gamma_Z}^2/{m_Z}^2} \tag{1}$$

where $s' = s - 2E_\gamma\sqrt{s}$, Γ_e is the Z^0 partial width to electrons and the total width, Γ_Z, can be expressed as

$$\Gamma_Z = \Gamma_{had} + \sum_{\ell=e,\mu,\tau} \Gamma_\ell + \Gamma_{inv} \tag{2}$$

with Γ_{inv} defined as

$$\Gamma_{inv} = N_\nu \Gamma_\nu \ . \tag{3}$$

The Z^0 partial widths to hadrons, charged leptons and one generation of massless neutrinos, denoted by Γ_{had}, Γ_ℓ, and Γ_ν, respectively, are set to their SM values calculated with m_Z = 91.187 GeV [29], m_{top} = 150 GeV and m_{higgs} = 100 GeV. All calculations use these central values for m_Z, m_{top} and m_{higgs}.

In a first step, we test the compatibility of the measured cross-sections with each integral N_ν hypothesis using the full $\nu\overline{\nu}\gamma(\gamma)$ cross-section calculation of [20]. We use a χ^2 test and combine the six data-points below the peak into three data-points to ensure reasonable statistics per bin. The correlated systematic errors on the efficiency, the background expectation and the predicted cross-section[9] are accounted for in the covariance matrix. One finds χ^2 values (for 12 degrees of freedom) of 79, 15 and 22 for the N_ν = 2, 3 and 4 hypotheses respectively. This indicates that the data exclude $N_\nu = 2$, are consistent with $N_\nu = 3$ and do not favour $N_\nu = 4$.

Within the above frame-work where the partial width for visible Z^0 decays is fixed to the SM value, variations of Γ_{inv} necessarily affect Γ_Z. The curves in Figure 9 with N_ν = 2, 3 and 4, correspond to models with values of Γ_Z differing by about 167 MeV. The N_ν = 2 and 4 hypotheses are therefore ruled out by the LEP lineshape measurements which have a precision on Γ_Z of 7 MeV [1, 2, 3] (0.3 %). It is interesting to note that the $N_\nu = 2$ and 4 hypotheses are also excluded, at least at the 95 % CL, based on the single photon cross-section alone.

In a second step, we shall determine Γ_{inv} directly from the single photon cross-section. As shown in equation (1), we need to specify m_Z, Γ_e, and Γ_Z. Given its high experimental precision, we shall fix Γ_Z to a value consistent with the measured value of 2.489 ± 0.007 GeV. In this approach with Γ_Z fixed, the single photon cross-section varies linearly with Γ_{inv} and is correspondingly more sensitive to Γ_{inv}. In addition to the expected dominant Z^0 resonant term described above, we need to assume something about the W contributions to the single photon cross-section. Our previous analysis [8] fixed the W terms to the SM values. In practice, this means that we assume the SM value of the electron axial-vector coupling and amounts to fixing the vector coupling of the electron to a value compatible with the assumed Γ_e. In addition, it should be noted that the W-Z interference contribution is calculated with the SM value of the Z^0 coupling to electron-type neutrinos.

We realise the above intention by computing the expected single photon cross-sections at each centre-of-mass energy using the Monte Carlo calculation of [20] with N_ν = 3. This

[9] This error source is discussed in detail below.

calculation is based on the SM value of the invisible width, $\Gamma_{\rm inv}^{SM}$. We then re-compute cross-sections (σ_{ZZ}) with the W-contributions ignored. The difference between the two cross-section estimates (σ_W) gives the W-contributions which we assume to have their SM value. We then fit the single photon cross-section measured at each centre-of-mass energy for $\Gamma_{\rm inv}$ as follows:

$$\sigma(\sqrt{s},\Gamma_{\rm inv}) = {\sigma_W}^{SM}(\sqrt{s}) + \frac{\Gamma_{\rm inv}}{\Gamma_{\rm inv}^{SM}}{\sigma_{ZZ}}^{SM}(\sqrt{s}).$$

We check the $\nu\overline{\nu}\gamma(\gamma)$ cross-section calculation of [20] by comparing it with the KORALZ generator [24] for a kinematic acceptance of $E_\gamma > 1.5$ GeV ; $|\cos\theta| < 0.7$. The KORALZ code includes the latest calculations of electro-weak corrections as calculated in the ZFITTER program [4]. The cross-sections agree to better than 1 % for centre-of-mass energies on and above the Z^0 mass as observed in previous studies [22, 23] with a larger acceptance ($E_\gamma > 0.5$ GeV ; $|\cos\theta| < 0.966$). Below the Z^0 peak, the calculations differ by about 3 %, which is nevertheless negligible compared with the statistical errors on the data. The SM values of $\Gamma_{\rm Z}$, $\Gamma_{\rm e}$ and $\Gamma_{\rm inv}$ calculated using the ZFITTER program, with α_S set to 0.12 (KORALZ default), are 2491, 83.8 and 500.8 MeV respectively. These central values for $\Gamma_{\rm Z}$ and $\Gamma_{\rm e}$ are in good agreement with experiment [1, 2, 3].

We use a maximum likelihood fit to the observed number of events at each of the fifteen centre of mass energies. The likelihood function contains Poisson probability distributions for the signal and background expectations. The former depends on $\Gamma_{\rm inv}$ according to the above cross-section, and the latter is listed in Table 5.

Besides the experimental systematic errors on the efficiency, normalisation and background subtraction, which affect the measured cross-section, interpreting the cross-section in terms of $\Gamma_{\rm inv}$ introduces some additional systematic uncertainties. We assign a 1 % theoretical error to the expected single photon cross-section justified by the above comparison of two independent calculations. The centre-of-mass energy scale uncertainties of the 1990, 1991 and 1992 data are 20, 6 and 18 MeV respectively [29, 30]. Based on an average uncertainty of 14 MeV on the centre-of-mass energy, one expects an uncertainty of 0.8 % on the invisible width. The experimental uncertainty on $m_{\rm Z}$ of 7 MeV [29] leads to a systematic uncertainty of 0.4 % on the predicted single photon cross-section.

The final result is

$$\Gamma_{\rm inv} = 539 \pm 26 \pm 17 \text{ MeV}$$

corresponding to

$$N_\nu = 3.23 \pm 0.16 \pm 0.10$$

where we have assumed the SM coupling of the Z^0 to neutrinos which gives a value for Γ_ν of 166.9 MeV per light neutrino generation when evaluated with $m_{\rm top} = 150$ GeV and $m_{\rm higgs} = 100$ GeV. The N_ν determination includes an additional systematic uncertainty of 0.5 % arising from varying the top quark mass between 100 and 200 GeV, and the Higgs mass between 60 GeV and 1 TeV. The difference between the measured cross-section and the expected cross-section for $N_\nu = 3$ is shown in Figure 10 and is compared with the best fit value of $N_\nu = 3.23$.

As noted previously, the above approach assumes the SM W contributions. The expectation without any W contributions is compared with the expectation using the full calculation in Figure 10. Despite some dependence of the W contributions on the centre-of-mass energy,

the main, but limited, discrimination between the two curves comes from the absolute cross-section at the Z^0 peak. We have fitted the single photon cross-sections as above but have also introduced a scale factor f_W, which scales the W cross-section contributions (so for SM, $f_W = +1$). We find, as expected, that f_W is very correlated with Γ_{inv}, and no meaningful independent conclusions on f_W can be drawn. In a second fit, we fix Γ_{inv} to the SM value of 500.8 MeV ($N_\nu = 3$), and fit for f_W. We find $f_W = 0.0 \pm 0.7 \pm 0.4$. This is consistent with $f_W = +1$ as expected, but also indicates that the present data can be described satisfactorily without any W contributions.

9 Limits on new physics from the total single photon cross-section

The comparison of the indirect method with this direct method of determining Γ_{inv} can be used to estimate the possible size of "exotic visible" Z^0 decays which are not selected by the standard visible decay analyses but contribute to the total width and hence the indirect invisible width but would not be sensed by the direct invisible width method. For the OPAL data [1], $\Gamma_{inv}(\text{lineshape}) - \Gamma_{inv}(\text{direct}) = -49 \pm 32$ MeV. The central value is outside the physical positive region. We use the method described in [31] to deal with this bound and set an upper limit at 95 % CL of 39 MeV on the partial width of the Z^0 to exotic visible processes.

The direct measurements of Γ_{inv} and N_ν can be used to set 95 % CL upper limits on these parameters of 593 MeV and 3.55, respectively. An additional heavy neutrino with standard couplings to the Z^0 would contribute $\frac{3}{4}\beta(1 + \beta^2/3)$ of a light neutrino generation, where β is the speed of the neutrino. Similarly, neglecting small effects from wino exchange, three generations of sneutrinos degenerate in mass would contribute $\frac{3}{2}\beta^3$ to N_ν (1.5 for $\beta = 1$). For the selected single photon sample, the average reduced centre-of-mass energy, $\sqrt{s'}$, estimated from the photon energy, is 88.4 GeV. This is consistent with the expectation of 88.5 GeV from the $\nu\overline{\nu}\gamma(\gamma)$ MC. Mass limits have been evaluated from the above upper limit on N_ν with β calculated for $\sqrt{s'} = 88$ GeV. We exclude an additional neutrino with mass lighter than 33 GeV at 95 % CL. Similarly, three generations of mass degenerate sneutrinos are excluded for masses below 30 GeV. The single photon data do not exclude one generation of light sneutrinos at the 95 % CL since the upper limit on N_ν exceeds 3.5.

Non-resonant sources of single photons can be investigated by fitting the data with the Standard Model expectation for $N_\nu = 3$ and an additional non-resonant component with cross-section independent of centre-of-mass energy. We find

$$\sigma_{\text{non-res}} = 1.3 \pm 0.7 \pm 0.4 \text{ pb}$$

corresponding to an upper limit at 95 % CL of 2.8 pb.

Similarly Z^0 decay contributions can be studied by fixing $N_\nu = 3$ and adding a component with the expected Z^0 lineshape. We use the measured $e^+e^- \rightarrow$ hadrons cross-sections at each centre-of-mass energy [1] to model the Z^0 lineshape and fit for the Z^0 partial width to invisible particle(s) and a single photon within the kinematic acceptance, Γ_{SP}, normalised to Γ_Z. The result is

$$\Gamma_{SP}/\Gamma_Z = (2.3 \pm 1.9 \pm 1.1) \times 10^{-5}$$

corresponding to an upper limit at 95 % CL of 6.2×10^{-5}. The upper limit on Z^0 decay to a single photon with energy exceeding 1.75 GeV in the angular region $|\cos\theta| < 0.7$ can be extended to the full solid angle. Assuming an isotropic angular distribution one calculates an upper limit on the Z^0 branching ratio to a single photon with energy exceeding 1.75 GeV of 8.7×10^{-5} at 95 % CL. Much more stringent, but more specific limits, can be obtained using the differential energy spectrum discussed in the next section.

10 Differential cross-section with photon energy

We present the differential cross-section with photon energy for single photon production, $d\sigma/dE_\gamma$. This is presented for data collected below the Z^0 peak, on peak and above the peak corresponding to average centre of mass energies of 89.29, 91.28 and 93.05 GeV with integrated luminosities of 3.5, 33.1 and 3.9 pb^{-1}, respectively. The total cross-section variation with $\sqrt{s}$ is approximately linear for the three $\sqrt{s}$ regions.

We proceed from the measured deposited energy spectrum of the 447 single photon candidates as follows. Firstly, we correct the deposited energy according to the expected energy loss for a photon with the observed $|\cos\theta|$ and deposited energy, such that the corrected energy is a good estimator of the actual photon energy. Secondly, we subtract the background contribution estimated for each bin of corrected energy. Thirdly, we estimate the efficiency for selecting a photon in the E_γ bin under consideration. The bin size is chosen to be typically about three times larger than the energy resolution. The efficiency, defined, as before, including feed-through, is found to be consistent with a constant value of $66.1 \pm 1.7\%$ for E_γ bins above 3 GeV, while it is 61.2 ± 0.6 % below 3 GeV, where the errors include only MC statistics[10]. The measured differential cross-section with photon energy for each combined centre-of-mass energy is shown in Table 7. Systematic errors on each bin are in general small compared to the statistical error. Based on the variation of efficiency from bin to bin, we assign a conservative error on the efficiency of 5 %. The uncertainty on the background estimates is about 25%. An overall energy scale error of 1 % contributes a typical uncertainty of 1–2 %.

The measured differential cross-sections are compared in Figure 11 with the expectations from the $\nu\overline{\nu}\gamma(\gamma)$ generator with $N_\nu = 3$. They agree reasonably well with the expectation. Below the peak, one sees that the somewhat higher than expected total cross-section arises principally from photon energies below 3 GeV. The shape of the energy spectrum is consistent with the expectation from initial state radiation. The on-peak data agree well with expectation over the complete energy range. Above the peak, there are indications of the expected shoulder at energies around $\sqrt{s} - m_Z$. The highest energy photon has an energy of 20.3 ± 0.8 GeV and is recorded at $\sqrt{s} \approx m_Z$.

On the Z^0 peak, nine events are observed with energy exceeding 10 GeV, compared with an expectation of 5.1 ± 0.5 events (4.8 ± 0.4 from $\nu\overline{\nu}\gamma(\gamma)$ and a background of 0.4 ± 0.2 from $\mu^+\mu^-\gamma$). Below the peak, two events are observed with photon energy exceeding 5 GeV, compared with an expectation of 3.0 ± 0.8 events. Above the peak, eight events have energy exceeding 5 GeV compared with an expectation of 5.9 ± 1.2 events. The latter expectations are dominated by

[10]The efficiency is lower below 3 GeV due to the effect of the deposited energy cut at 1.5 GeV.

E_γ range (GeV)	$\sqrt{s} < m_Z$	$\sqrt{s} \approx m_Z$	$\sqrt{s} > m_Z$
(1.75,2.25)	9.1 ± 3.2	8.7 ± 1.0	24.0 ± 4.7
(2.25,3.0)	4.1 ± 1.6	5.3 ± 0.6	20.7 ± 3.4
(3.0,4.0)	0.8 ± 0.6	1.7 ± 0.3	8.4 ± 1.8
(4.0,5.0)	0.8 ± 0.6	1.0 ± 0.2	5.0 ± 1.4
(5.0,6.0)		0.3 ± 0.1	0.3 ± 0.4
(6.0,8.0)	0.4 ± 0.3	0.2 ± 0.07	1.3 ± 0.5
(8.0,10.0)		0.09 ± 0.05	
(10.0,12.5)		0.034 ± 0.026	
(12.5,15.0)		0.032 ± 0.026	
(15.0,17.5)		0.037 ± 0.026	
(17.5,20.0)		0.037 ± 0.026	
(20.0,22.5)		0.018 ± 0.018	
(22.5,25.0)			
(25.0,50.0)			

Table 7: Differential cross-section with photon energy, $\mathrm{d}\sigma/\mathrm{d}E_\gamma$, in units of picobarn/GeV for the three combined scan-points with average centre-of-mass energies of 89.29 GeV, 91.28 GeV and 93.05 GeV. Only the statistical errors from the event counting are given in the table. Cells with no entries contain no observed events.

the $\nu\overline{\nu}\gamma(\gamma)$ process. Therefore one can conclude that the high energy part of the spectrum is in good agreement with the expectation from $\nu\overline{\nu}\gamma(\gamma)$ production.

Upper limits

Several possible sources of new physics can lead to events with a high energy single photon. Rather than discussing details of the parameter spaces of various models, we present upper limits on the single photon cross-section, integrated over the $|\cos\theta| < 0.7$ angular region, for various minimum photon energy requirements.

Upper limits on the integrated cross-section, $\sigma(E_\gamma > E_{\mathrm{min}}; |\cos\theta| < 0.7)$ are calculated for various E_{min} based on the number of observed photons with corrected energy exceeeding $E_{\mathrm{min}} - 3\delta_E$, where δ_E is the photon energy resolution. These limits are therefore also valid for mono-chromatic photon production with energy E_{min}. The efficiency is reduced by 5 % to account for systematic errors. The limit is set taking into account the expected background[11] from $\mathrm{e^+e^-} \to \nu\overline{\nu}\gamma(\gamma)$ with $N_\nu = 3$ and the known background processes with visible reaction products using the techniques discussed in [31]. These 95 % CL upper limits are displayed in Figure 12 for the three combined scan-points. The 95 % CL upper limit on the cross-section at the $\mathrm{Z^0}$ peak for production of a single photon with energy exceeding 23 GeV is found to be 0.15 pb. For models in which the photon could arise from $\mathrm{Z^0}$ decay, this limit is equivalent to a $\mathrm{Z^0}$ branching ratio limit to a photon with energy exceeding 23 GeV in the $|\cos\theta| < 0.7$ angular

[11] Poisson (Gaussian) statistics are used for intervals with less than (at least) 25 observed events. In cases where the background subtracted number of events is negative (or positive by less than one standard deviation for the Gaussian case), the background expectation is set equal to the observed number of events (Poisson case), or evaluated in the physical region (Gaussian case).

region of 3.3×10^{-6}. Strictly, this limit has been evaluated for the angular distribution expected of single photons from initial state radiation. However, it is insensitive to this assumption. As an example, for an extreme angular distribution of $\sin^2\theta$, the acceptance would be only 1.5% lower than for the angular distribution expected for initial state radiation. This limit, in the restricted $|\cos\theta|$ range, can be extended to the full solid angle if one knows the relevant angular distribution. Assuming an isotropic angular distribution, one can set an upper limit on the Z^0 branching ratio to a single photon of energy exceeding 23 GeV of 4.7×10^{-6} corresponding to a Z^0 partial width of 11 keV.

As an example of a model constrained by this limit, we consider the variant axion model [12]. In this model, the decay constant, F_a, is of order 10 GeV leading to an axion with mass of order 1 MeV which would decay outside the detector. The small mass of the axion means that the single photon would be produced with the beam energy.

Search for γX production

A new particle X may be produced in association with a photon. For example, the Z^0 can decay to $H^0\gamma$ at the one loop level for $m_{\rm higgs} < m_Z$. In addition, if particle X were to couple to two photons (possible for the Higgs), then it could also be produced through s-channel photon exchange. These production mechanisms, in the case of the Higgs, are expected to be suppressed in most minimal models compared to the more abundant Bjorken process, but in some extensions, such as [32], they can be substantially enhanced. If particle X is invisible or can decay invisibly, then it could be seen in the single photon topology. This could happen for example for the production of a $Z^{0\prime}$, variant axion, "invisible" Higgs or $Z^0 \to \tilde{\nu}\gamma$ in supersymmetric models with explicit R-parity violation [33].

We study the distribution of the mass of the system recoiling against the photon ($M_{\rm recoil}$, the recoil mass), and use the corrected energy as discussed above. For single photon emission in the initial state, $M_{\rm recoil}$ is equivalent to $\sqrt{s'}$, the reduced centre-of-mass energy. The recoil mass distribution is shown in Figure 13(a) for the single photon candidates. It is consistent with that expected from known sources. In order to calculate an upper limit on the γX production cross-section for a specified mass of X with a photon produced in the angular region $|\cos\theta| < 0.7$, we scan through all possible mass values. We accept events as candidates if they are within three standard deviations of the mass value. The recoil mass resolution is calculated directly from the photon energy resolution. The procedure assumes that the width of particle X is small compared to the mass resolution. The efficiency is estimated as in the previous section, and we include data from all centre-of-mass energies. The cross-section upper limit at 95 % CL for the restricted angular range is shown in Figure 13(b). The limit takes into account the expected background from $\nu\overline{\nu}\gamma(\gamma)$ with $N_\nu = 3$ and the background from visible processes. The upper limit for $m_X < 64$ GeV is 0.12 pb and for $m_X < 84$ GeV it is 0.4 pb. Assuming an isotropic angular distribution, one can integrate over the full solid angle to obtain cross-section upper limits for the two mass intervals specified above of 0.2 pb and 0.65 pb corresponding to Z^0 branching ratios to a photon and particle X with an invisible signature of 4.3×10^{-6} and 1.4×10^{-5} respectively.

11 Summary

A measurement of the single photon production cross-section is presented based on a data-sample of 40.5 pb^{-1} collected with the OPAL detector at centre-of-mass energies within 3 GeV of the Z^0 resonance. A total of 447 single photon candidates were observed with energy exceeding 1.75 GeV in the polar angle region $|\cos\theta| < 0.7$. The estimated background from visible reaction products is 37.1 ± 6.2 events. After subtraction of expected background events, the centre-of-mass energy dependence of the measured single photon cross-section is found to be consistent with expectations from Standard Model contributions arising from Z^0 decay to three light neutrino generations and W-exchange contributions for electron-type neutrinos.

Interpreting the cross-sections as being solely due to Z^0 decay to invisible particles and the expected W-contributions, the Z^0 invisible width, $\Gamma_{\rm inv}$, is determined to be $539 \pm 26 \pm 17$ MeV corresponding to $N_\nu = 3.23 \pm 0.16 \pm 0.10$ effective light neutrino generations. On the other hand, if one fixes the Z^0 exchange contribution to that expected for $N_\nu = 3$ then one observes that the data are consistent with the expected contributions from W-exchange and W-Z interference. However, the data can be described satisfactorily without such contributions.

This direct measurement of the invisible width fully saturates the indirect measurement from the Z^0 line-shape thus limiting possible exotic Z^0 decays to visible particles which might escape classification by the standard di-lepton and multi-hadronic event analyses. We infer an upper limit of 39 MeV at 95 % CL on such an exotic visible partial width. All of the following limits are given at this confidence level.

The measurement of $\Gamma_{\rm inv}$, and correspondingly N_ν, leads to upper limits on these parameters of 593 MeV and 3.55 respectively. This excludes, by a direct search, an additional neutrino with mass lighter than 33 GeV.

Additional contributions to the single photon cross-section from non-resonant production, namely initial state radiation and the non-resonant production of an invisible final state, or of single photons produced in association with invisible particles(s) in Z^0 decay, are constrained by the cross-section data. By fitting these data to the Standard Model expectation for $\nu\overline{\nu}\gamma(\gamma)$ production plus the additional contribution, we set an upper limit on a non-resonant component of 2.8 pb and an upper limit on the Z^0 branching ratio to a single photon of energy exceeding 1.75 GeV of 8.7×10^{-5}, where in the latter limit we have assumed an isotropic angular distribution. The Z^0 branching ratio upper limit for $|\cos\theta| < 0.7$ is 6.2×10^{-5} with no angular distribution assumptions.

The differential cross-section with photon energy of single photon production is presented for three centre-of-mass energy intervals and is consistent with Standard Model expectations for $\nu\overline{\nu}\gamma(\gamma)$ production. No anomalous high energy photon production is observed. The most energetic single photon event observed has a photon energy of 20.3 ± 0.8 GeV. Upper limits on the cross-section at each centre-of-mass energy interval are given for the angular range $|\cos\theta| < 0.7$ for arbitrary minimum energy exceeding 1.75 GeV. The upper limit at the Z^0 peak on production of a single photon with energy exceeding 23 GeV corresponds to a Z^0 branching ratio limit of 3.3×10^{-6} within the angular acceptance.

The distribution of the mass recoiling against the single photon shows no obvious resonance structure. The cross-section, within $|\cos\theta| < 0.7$, for radiative decay of a virtual photon or

Z^0 to a new particle X of mass less than 64 GeV and with an invisible signature is limited to 0.12 pb and equivalently for masses less than 84 GeV the upper limit is 0.4 pb. These upper limits can be interpreted as limits on the Z^0 branching ratio of 4.3×10^{-6} and 1.4×10^{-5} for a new particle X in the above mass ranges.

Acknowledgements

We thank Z. Wąs for useful discussions and F. Linde for his help with the $e^+e^- \to e^+e^-\ell^+\ell^-\gamma$ Monte Carlo generator. It is a pleasure to thank the SL Division for the efficient operation of the LEP accelerator, the precise information on the absolute energy, and their continuing close cooperation with our experimental group. In addition to the support staff at our own institutions we are pleased to acknowledge the
Department of Energy, USA,
National Science Foundation, USA,
Particle Physics and Astronomy Research Council, UK,
Natural Sciences and Engineering Research Council, Canada,
Fussefeld Foundation,
Israel Ministry of Science,
Israel Science Foundation, administered by the Israel Academy of Science and Humanities,
Minerva Gesellschaft,
Japanese Ministry of Education, Science and Culture (the Monbusho) and a grant under the Monbusho International Science Research Program,
German Israeli Bi-national Science Foundation (GIF),
Direction des Sciences de la Matière du Commissariat à l'Energie Atomique, France,
Bundesministerium für Forschung und Technologie, Germany,
National Research Council of Canada,
A.P. Sloan Foundation and Junta Nacional de Investigação Científica e Tecnológica, Portugal.

References

[1] OPAL Collab., R. Akers et al., Z. Phys. **C61** (1994) 19.

[2] ALEPH Collab., D. Buskulic et al., CERN-PPE/94-30, submitted to Z. Phys. **C** ;
DELPHI Collab., P. Abreu et al., Nucl. Phys. **B418** (1994) 403 ;
L3 Collab., M. Acciarri et al., CERN-PPE/94-45, submitted to Z. Phys. **C**

[3] The LEP Collaborations, CERN-PPE/93-157, Aug. 1993.

[4] D. Bardin et al., CERN-TH.6443/92.

[5] A.D. Dolgov, L.B. Okun and V.I. Zakharov, Nucl. Phys. **B41** (1972) 197;
E. Ma and J. Okada, Phys. Rev. Lett. 41 (1978) 287;
K.J.F. Gaemers, R. Gastmans and F.M. Renard, Phys. Rev. **D19** (1979) 1605;
G. Barbiellini, B. Richter and J.L. Siegrist, Phys. Lett. **B106** (1981) 414.

[6] G.V. Borisov, V.N. Larin and F.F. Tikhonin, Z. Phys. **C41** (1988) 287.

[7] MAC Collab., W.T. Ford et al., Phys. Rev. **D33** (1986) 3472;
H. Wu, Ph.D Thesis, Univ. Hamburg, 1986;
CELLO Collab., H.-J. Behrend et al., Phys. Lett. **B215** (1988) 186;
ASP Collab., C. Hearty et al., Phys. Rev. **D39** (1989) 3207;
VENUS Collab., K. Abe et al., Phys. Lett. **B232** (1989) 431.

[8] OPAL Collab., M. Z. Akrawy et al., Z. Phys. **C50** (1991) 373.

[9] L3 Collab., B. Adeva et al., Phys. Lett. **B275** (1992) 209;
L3 Collab., O. Adriani et al., Phys. Lett. **B292** (1992) 463;
ALEPH Collab., D. Buskulic et al., Phys. Lett. **B313** (1993) 520.

[10] J.D. Ware and M.E. Machacek, Phys. Lett. **B147** (1984) 415.

[11] C. Jarlskog, Phys. Lett. **B241** (1990) 579.

[12] J.E. Kim and U.W. Lee, Phys. Lett. **B233** (1989) 496.

[13] L. Randall and E.H. Simmons, Nucl. Phys. **B380** (1992) 3.

[14] D.A. Dicus, S. Nandi and J. Woodside, Phys. Lett. **B258** (1991) 231.

[15] L3 Collab., O. Adriani et al., Phys. Lett. **B297** (1993) 469;
L3 Collab., O. Adriani et al., Phys. Rep. 236 (1993) 1;
ALEPH Collab., D. Decamp et al., Phys. Rep. **V216** (1992) 253;
OPAL Collab., M.Z. Akrawy et al., Phys. Lett. **B248** (1990) 211;
OPAL Collab., M.Z. Akrawy et al., Phys. Lett. **B251** (1990) 211.

[16] OPAL Collab., K. Ahmet et al., Nucl. Instrum. and Meth. **A305** (1991) 275.

[17] P.P. Allport et al., Nucl. Instrum. and Meth. **A324** (1993) 34.

[18] M. Arignon et al., Nucl. Instrum. and Meth. **A313** (1992) 103.

[19] J. Allison et al., Nucl. Instrum. and Meth. **A317** (1992) 47.

[20] F. A. Berends et al., Nucl. Phys. **B301** (1988) 583;
R. Miquel, C. Mana and M. Martinez, Z. Phys. **C48** (1990) 309.

[21] OPAL Collab., P. D. Acton et al., Phys. Lett. **B288** (1992) 373.

[22] L. Trentadue et al. in "Z Physics at LEP1", G. Altarelli ed., CERN 89-08 (1989) 129.

[23] P. Colas, R. Miquel and Z. Wąs, Phys. Lett. **B246** (1990) 541.

[24] S. Jadach, B.F.L. Ward and Z. Wąs, Comp. Phys. Comm. 66 (1991) 276.

[25] D. Karlen, Nucl. Phys. **B289** (1987) 23.

[26] F. A. Berends and R. Kleiss, Nucl. Phys. **B186** (1981) 22.

[27] A. Buijs et al., Comp. Phys. Comm. 79 (1994) 523.

[28] R. Kleiss, Phys. Lett. **B180** (1986) 400.

[29] LEP Energy Group and the LEP Collaborations, L. Arnaudon et al., Phys. Lett. **B307** (1993) 187.

[30] V. Hatton et al., "LEP Absolute Energy in 1990", LEP Perf. Note 12 (Dec. 1990), unpublished;
L. Arnaudon et al., "Energy Calibration of LEP in 1991", CERN SL/92-37, July 1992;
L. Arnaudon et al., "Energy Calibration of LEP in 1992", CERN SL/93-21, April 1993.

[31] Particle Data Group, K. Hikasa et al., Phys. Rev. **D45** (1992) 1.

[32] K. Hagiwara, R. Szalapski and D. Zeppenfeld, Phys. Lett. **B318** (1993) 155.

[33] J. L. Hewett in "Workshop on Photon Radiation from Quarks", S. Cartwright ed., CERN 92-04 (1992) 201.

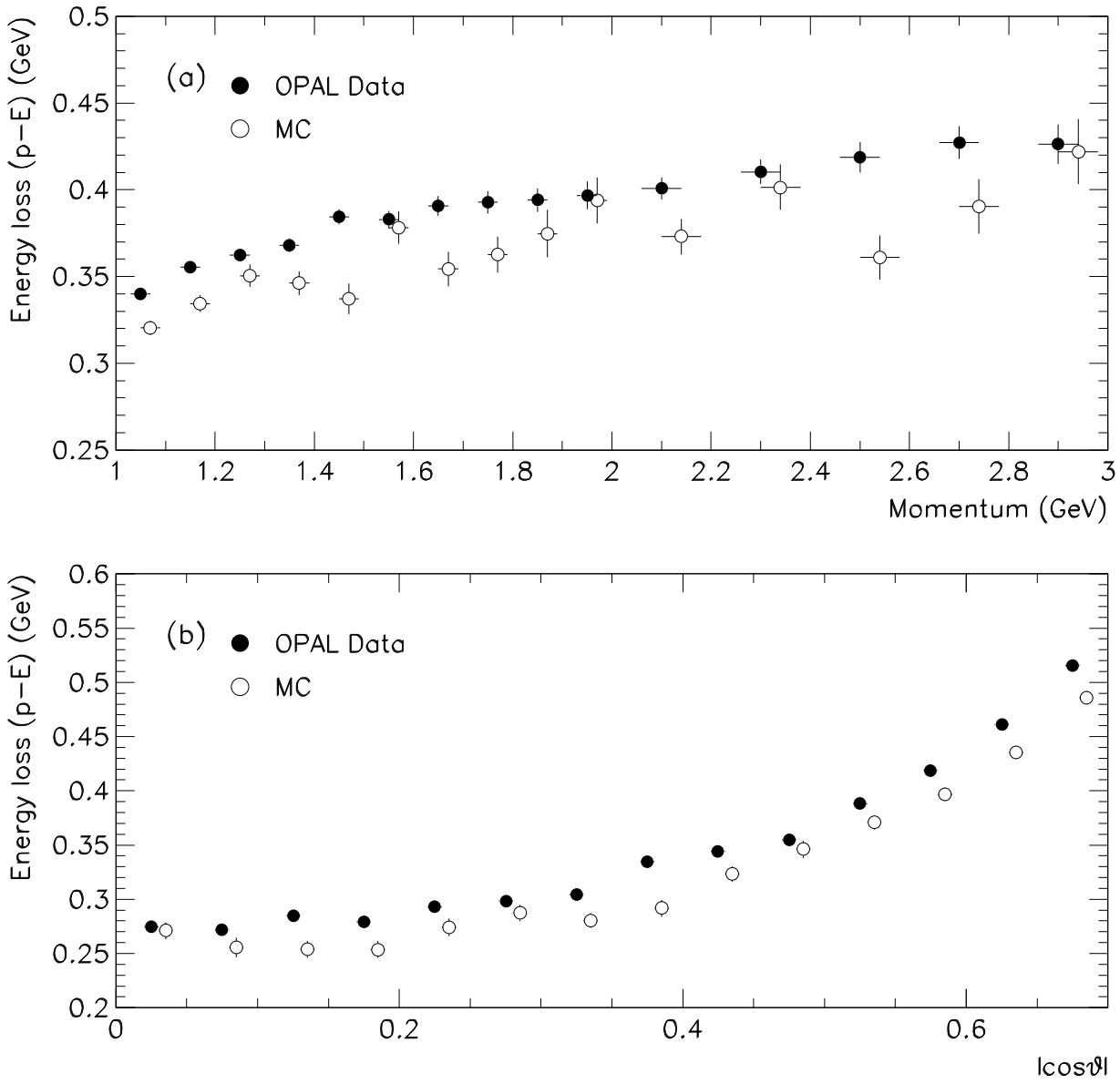

Figure 1: Results of Gaussian fits to the distribution of "energy loss" measured for single electron events for bins in (a) electron momentum and (b) $|\cos\theta|$. Energy loss is defined as $p - E$ where p is the electron momentum and E the associated deposited energy in the electromagnetic calorimeter. Solid points - data, open circles - MC.

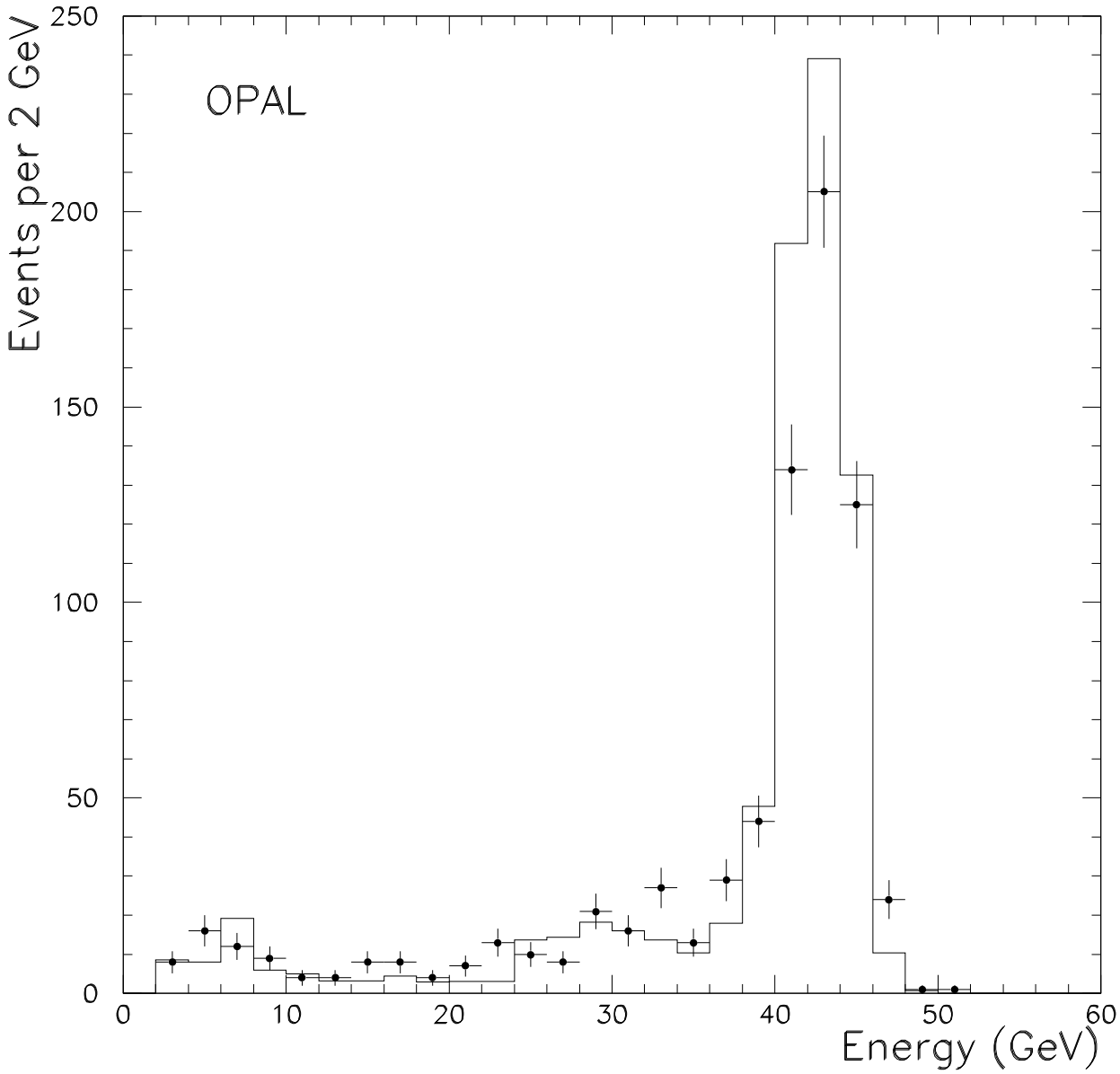

Figure 2: Energy measured in the forward calorimeter with the highest energy for the 751 events rejected only by criterion C2. The data are represented by points with error bars and the Monte Carlo expectation is shown as the histogram. Monte Carlo expectations for the signal process and the first five background processes listed in Table 3 are included.

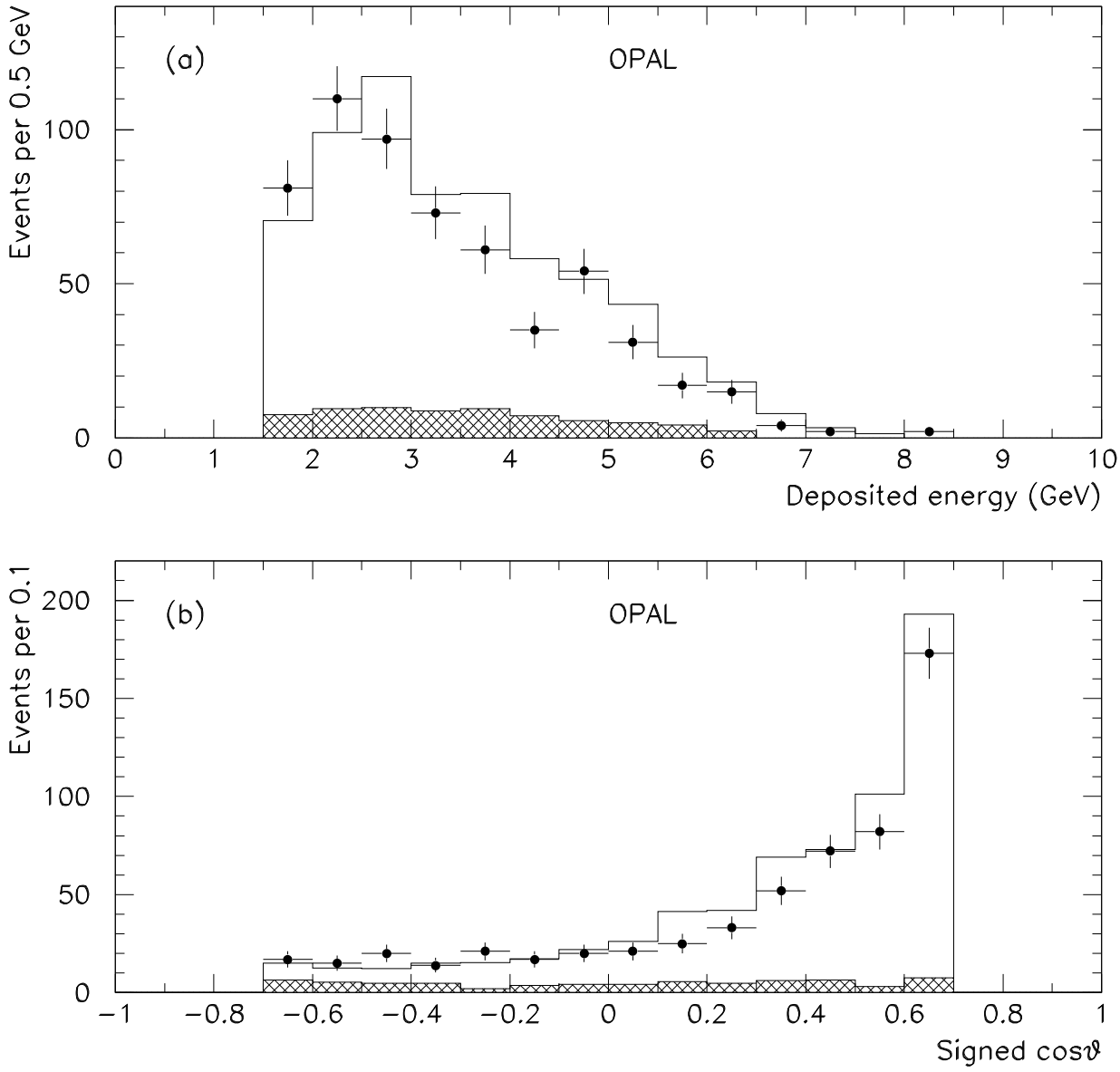

Figure 3: Barrel photon distributions for single photon events with a forward detector single tag as described in the text. (a) Deposited energy (b) signed $\cos\theta$. The $\cos\theta$ distribution is signed positively when the tag is in the same hemisphere in z as the photon and negatively otherwise. Monte Carlo expectations for $e^+e^- \to e^+e^-\gamma$ (unshaded part of histogram) and $e^+e^- \to \gamma\gamma\gamma$ (shaded) are superimposed. The MC statistical errors are slightly smaller than those of the data.

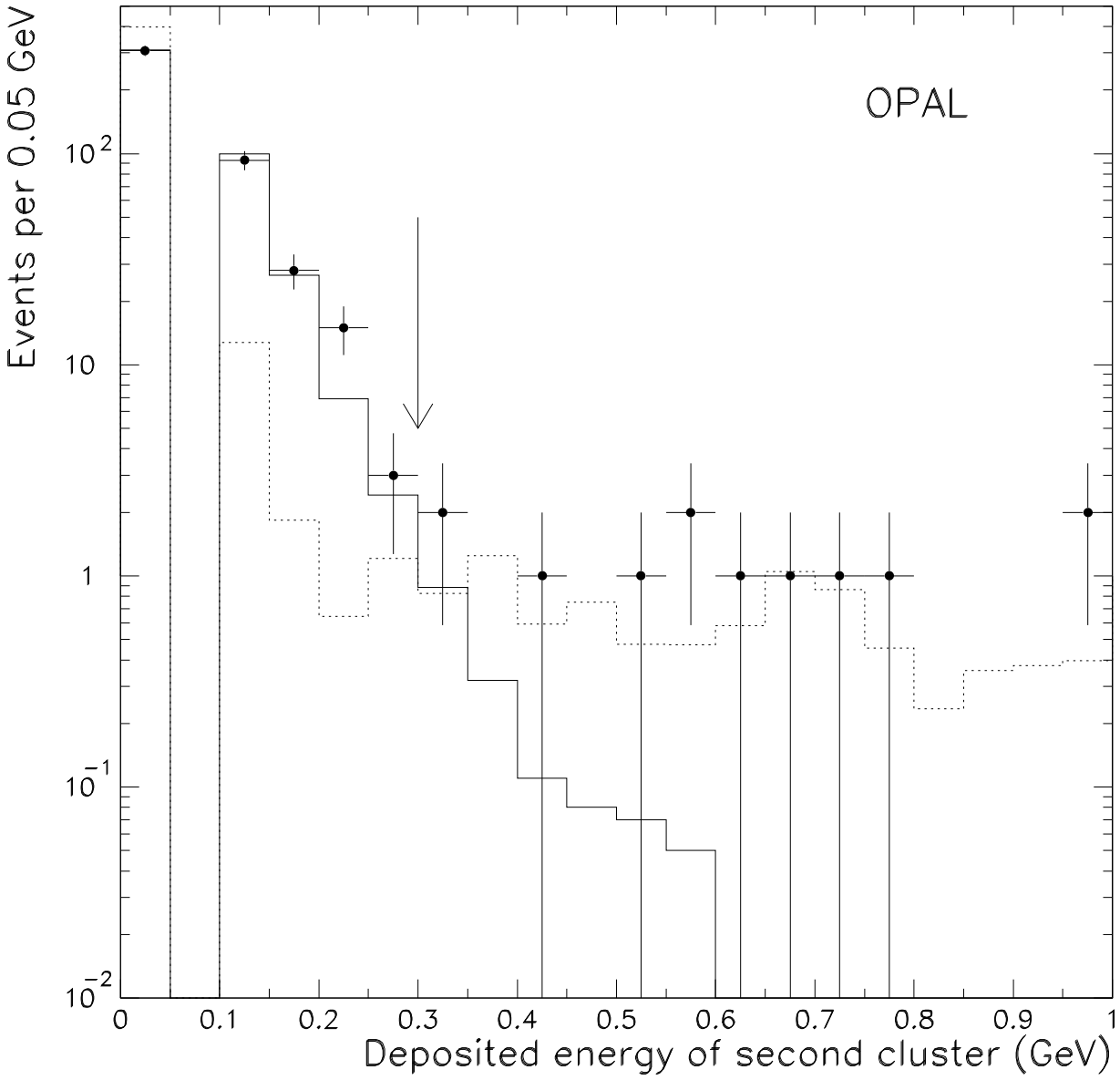

Figure 4: Energy of the second most energetic electro-magnetic cluster in the event for selected single photon candidates, and events failing exclusively on criterion C1. A total of 408 events are removed by criterion C1 based on a second cluster with energy exceeding 1 GeV and are not displayed in this figure. The data are represented by points with error bars and the full-line histogram represents the energy distribution measured with unbiased bunch crossing triggers. The dashed-line histogram shows the expectation from the simulated processes (mostly $\nu\bar{\nu}\gamma\gamma$). The first bin shows the number of events with no other cluster above 100 MeV. The arrow shows the position of the cut (C1).

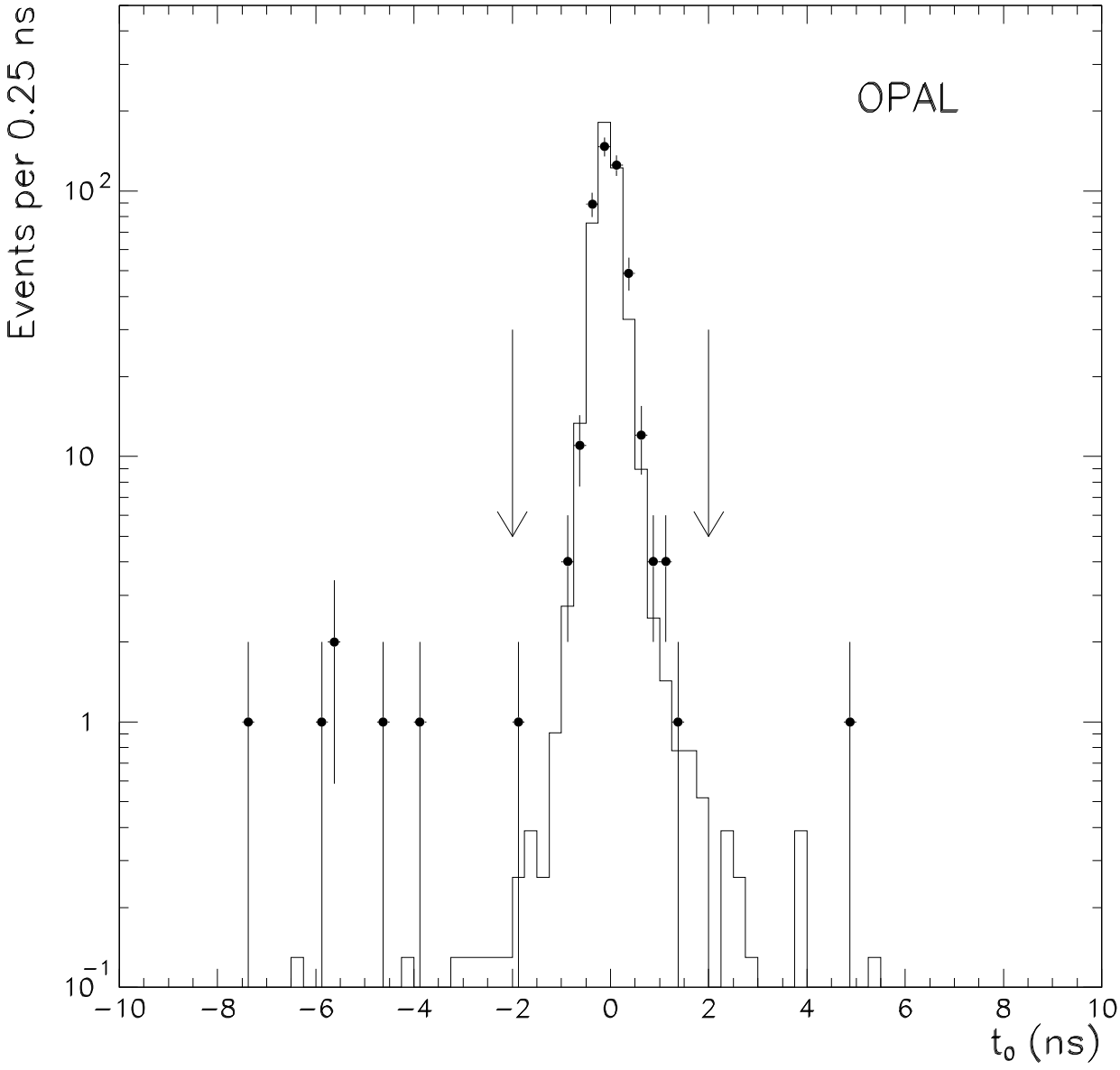

Figure 5: t_0 distribution for single photon candidates (data-points) compared to photons from the photon control sample (histogram). The arrows mark the positions of the timing cut (A3).

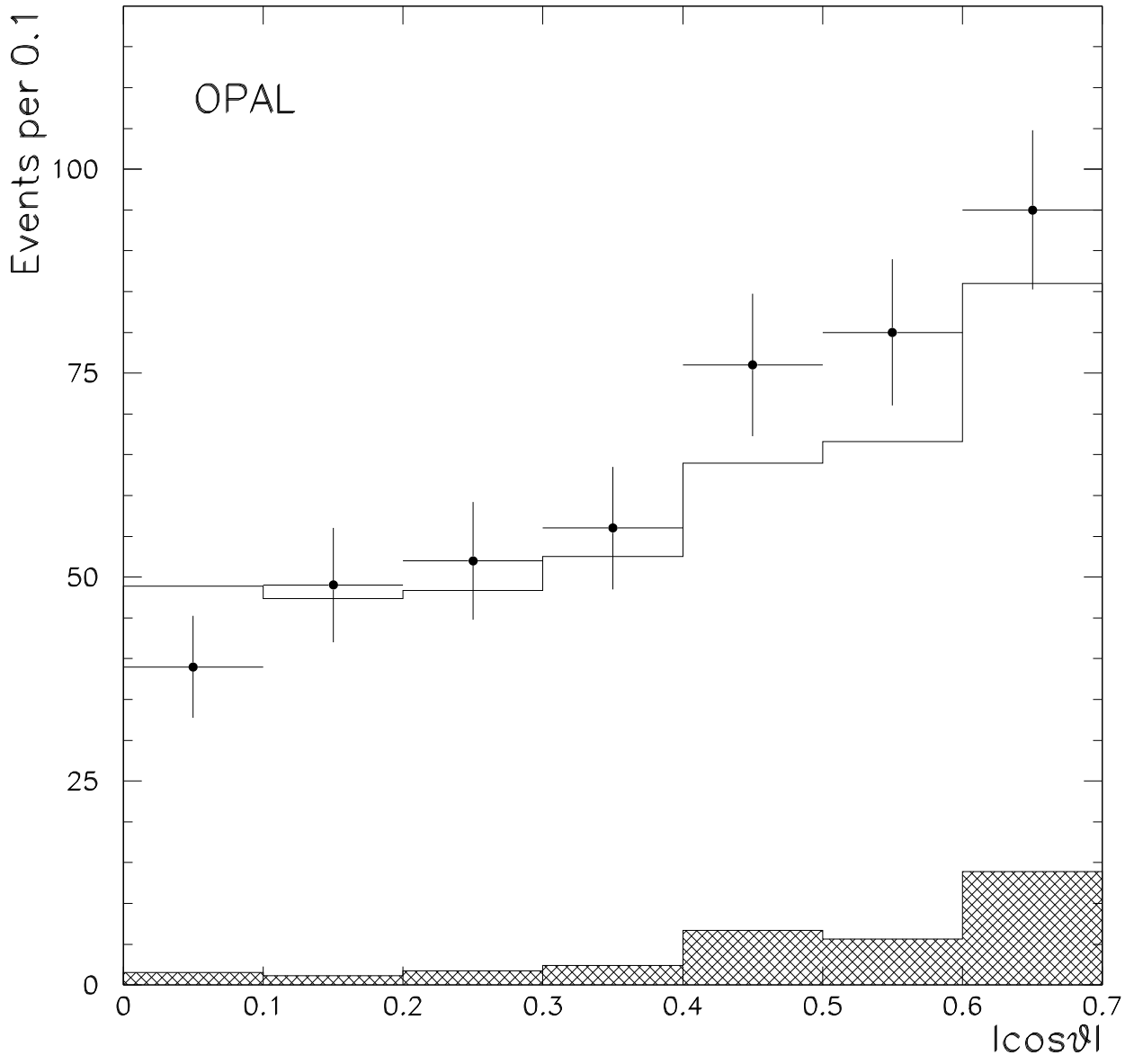

Figure 6: $|\cos\theta|$ distribution for the single photon candidates (points with error bars) compared to the expectation from the estimated background processes (shaded histogram) plus the expectation for $\nu\overline{\nu}\gamma(\gamma)$ production with $N_\nu = 3$ (unshaded part of the histogram).

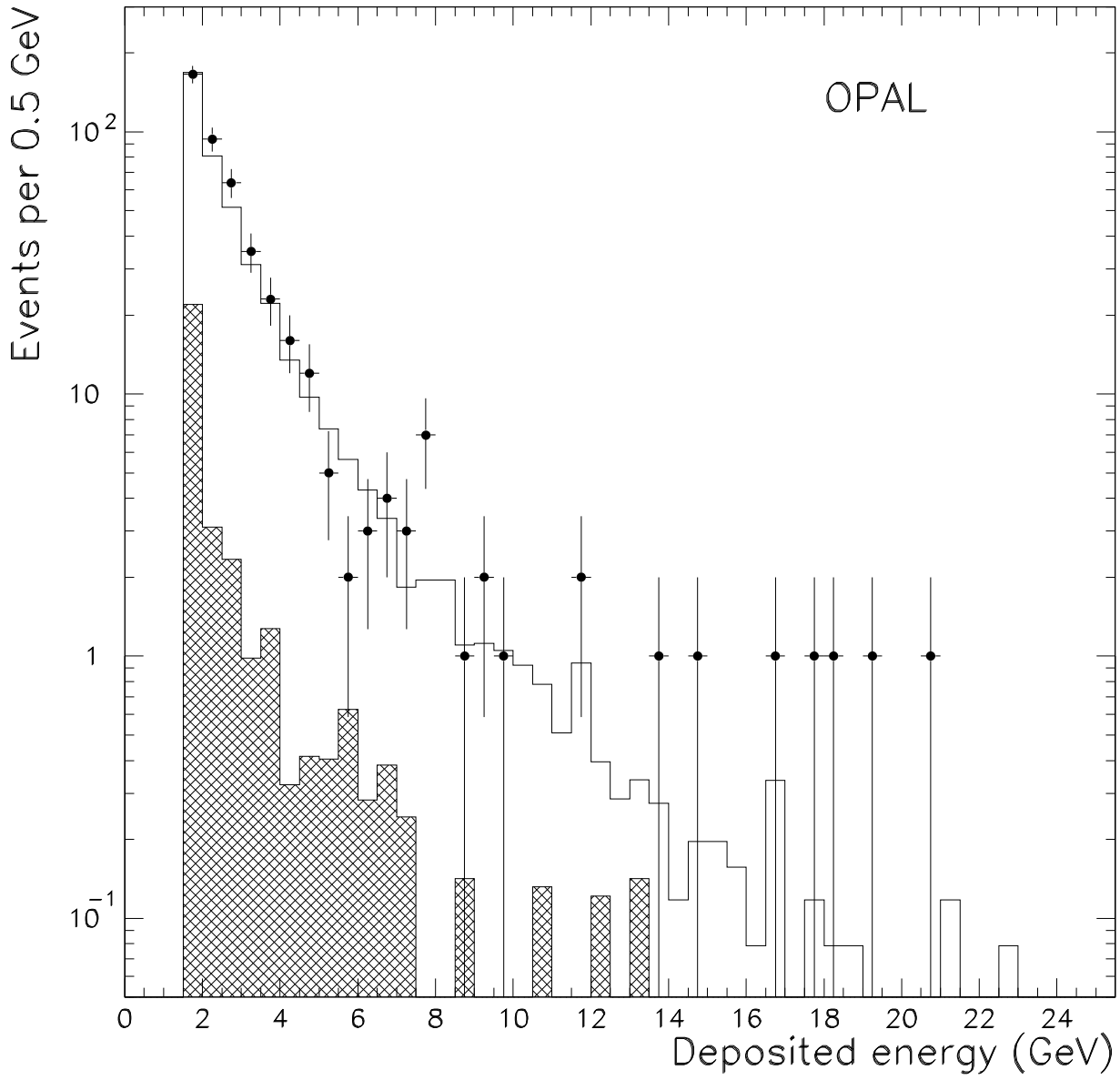

Figure 7: Deposited energy distribution shown on a logarithmic scale for single photon candidates (points with error bars) compared to the expectation from the estimated background processes (shaded histogram) plus the expectation for $\nu\overline{\nu}\gamma(\gamma)$ production with $N_\nu = 3$ (unshaded part of the histogram).

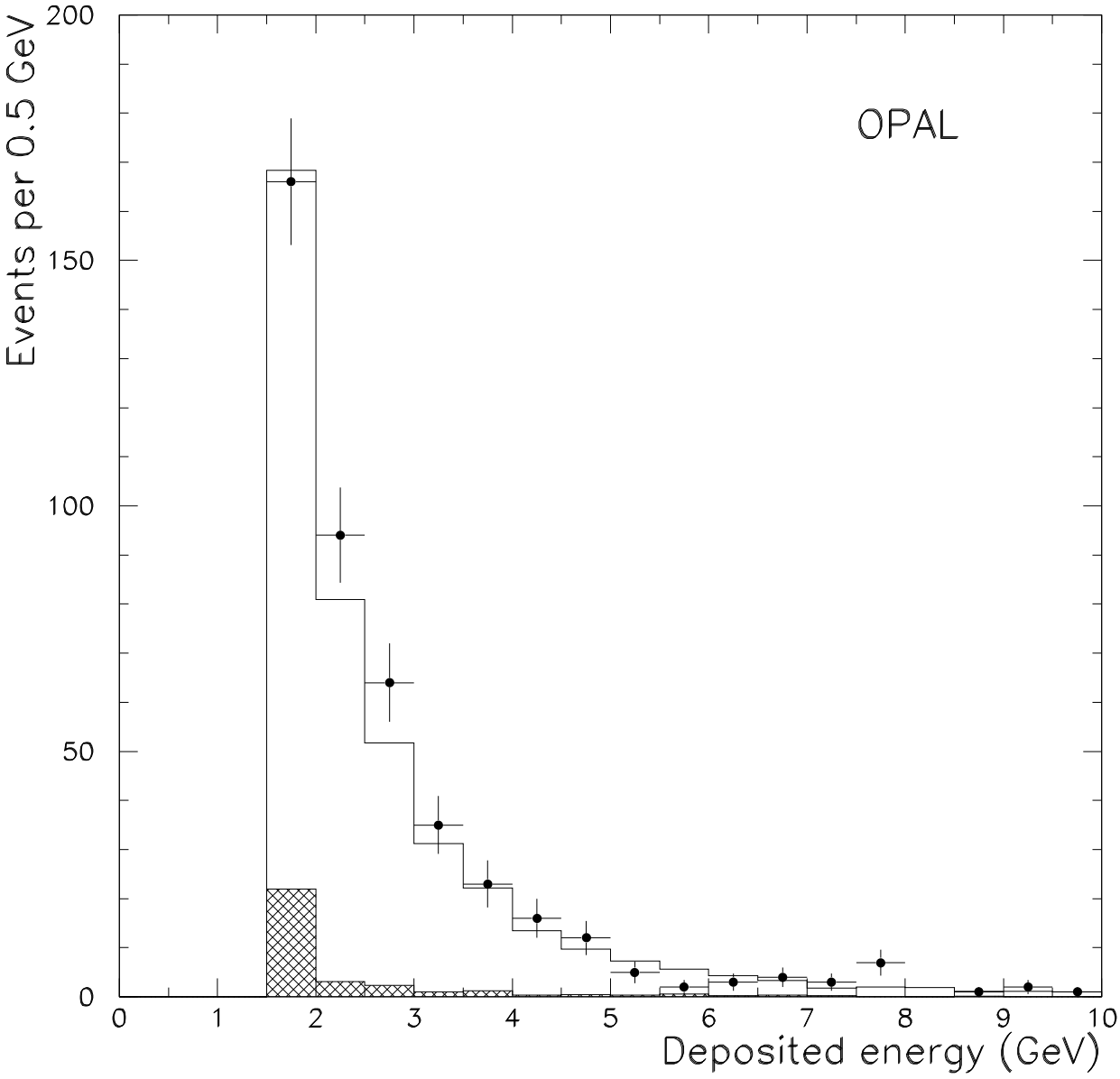

Figure 8: Deposited energy distribution shown on a linear scale for single photon candidates (points with error bars) compared to the expectation from the estimated background processes (shaded histogram) plus the expectation for $\nu\overline{\nu}\gamma(\gamma)$ production with $N_\nu = 3$ (unshaded part of the histogram).

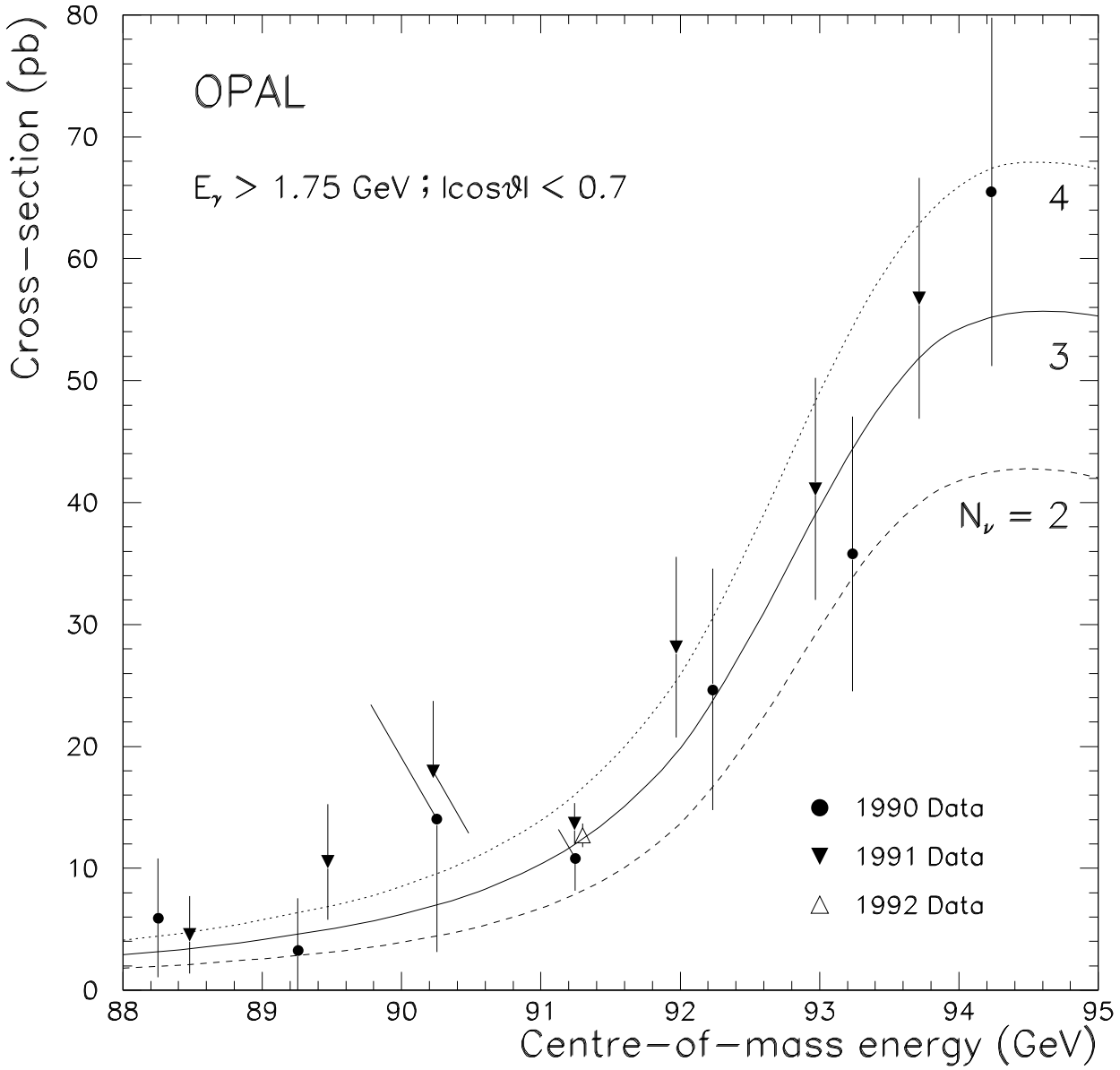

Figure 9: Measured cross-section for single photon production after subtraction of expected background processes at each data-taking point compared with the theoretical expectations for two, three and four light neutrino generations. The curves are calculated with the generator of [20] with parameters as described in the text. In this calculation, Γ_Z increases by 167 MeV per light neutrino generation.

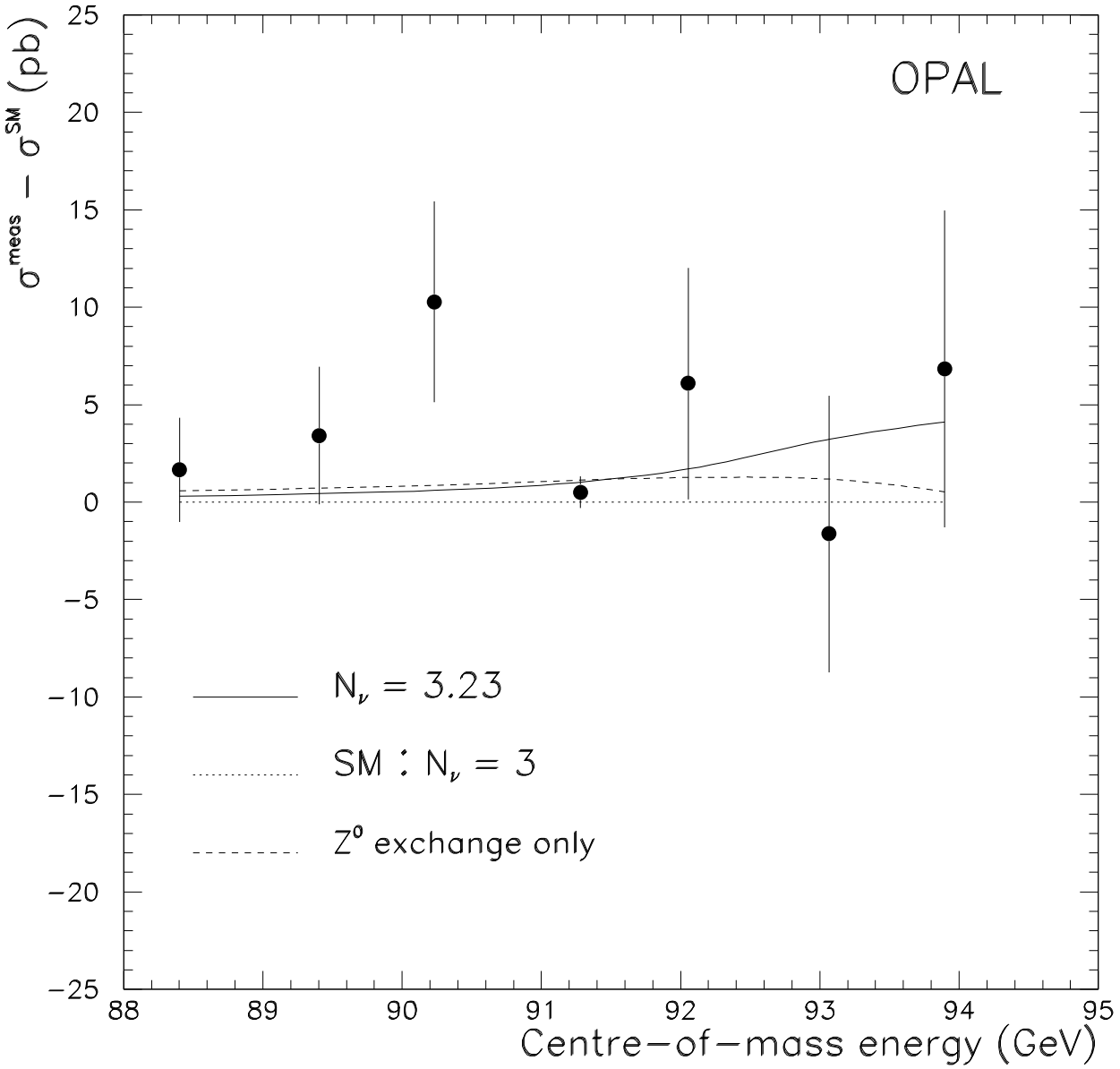

Figure 10: Measured cross-section for single photon production minus the expected cross-section evaluated for $N_\nu = 3$. The full line indicates the fitted central value of $N_\nu = 3.23$. The Standard Model expectation for $N_\nu = 3$ is the dotted line at zero, while the dashed line indicates the expectation neglecting any W contributions (Z^0 exchange only). Adjacent centre-of-mass energies have been combined.

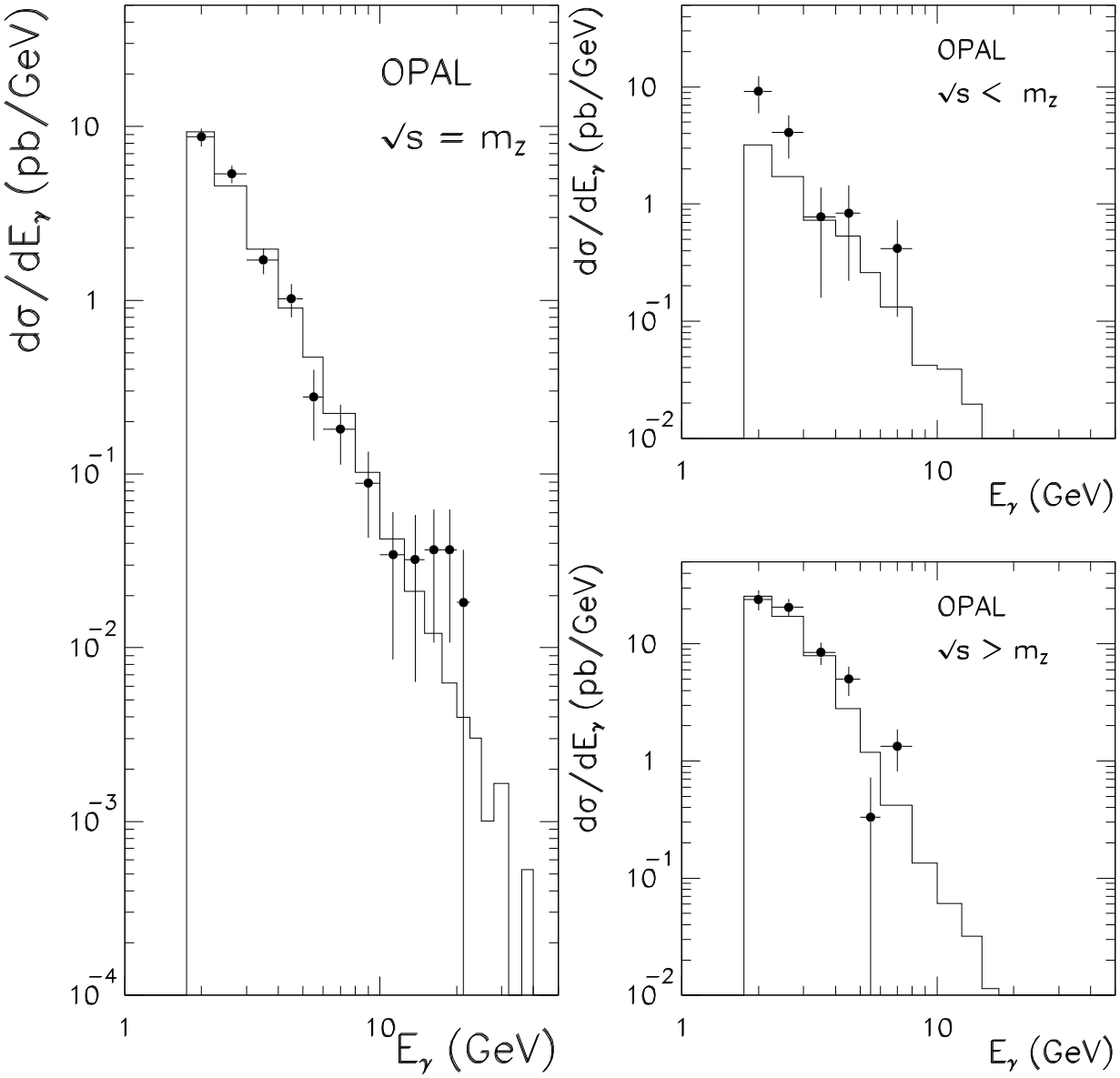

Figure 11: Measured differential cross-section with photon energy for single photon production after subtraction of expected background processes at each combined energy scan-point. The data (points with error bars) are compared with the expectation (histogram) with $N_\nu = 3$. The integrated luminosity of the MC expectation is 150 times that of the data, and all fifteen centre-of-mass energy points are included with their correct luminosity weight.

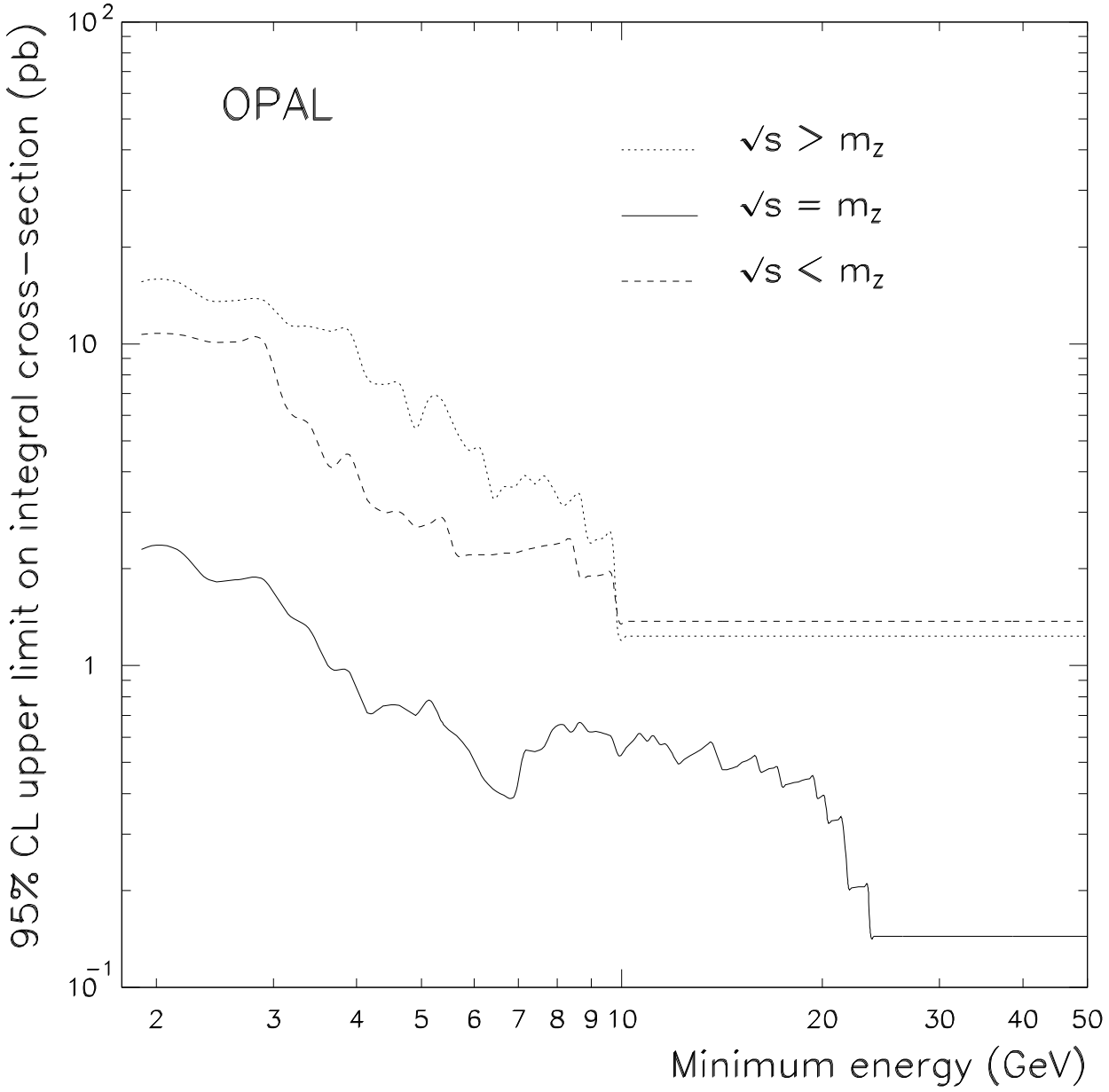

Figure 12: Upper limits at 95% CL on the cross-section for single photon production in the angular range $|\cos\theta| < 0.7$ integrated over the photon energy from a specified minimum energy up to the kinematic limit. The cross-section limits are presented for the three combined scan points with average centre-of-mass energies of 89.29, 91.28, 93.05 GeV. The upper limits are calculated taking into account the Standard Model expectation for $\nu\overline{\nu}\gamma(\gamma)$ with $N_\nu = 3$ and the known background processes.

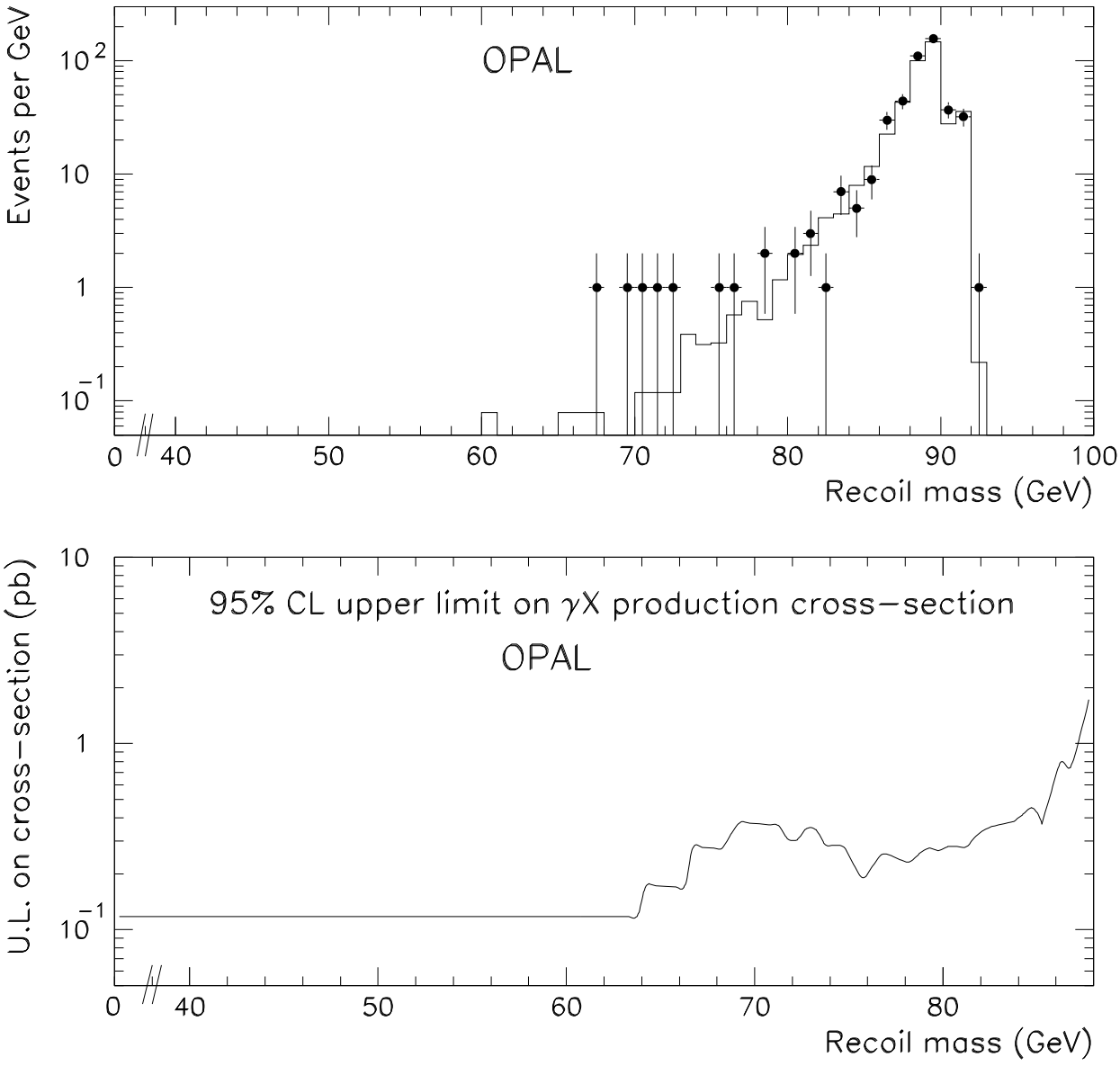

Figure 13: The upper plot shows the recoil mass of the 447 single photon candidates (points with error bars) compared to the expectation for $\nu\overline{\nu}\gamma(\gamma)$ with $N_\nu = 3$ and the known background processes (histogram). The lower plot shows the upper limit at 95% CL on the cross-section for production of a single photon within the angular range $|\cos\theta| < 0.7$ in association with a particle X which decays invisibly, for a range of values of the mass of particle X. The cross-section limit is based on 40.5 pb^{-1} of integrated luminosity collected at several centre-of-mass energies near the Z^0 peak. The upper limit is calculated taking into account the Standard Model expectation for $\nu\overline{\nu}\gamma(\gamma)$ with $N_\nu = 3$ and the known background processes. No events are observed with recoil mass below 40 GeV. The limit extends to zero mass.